From late-Variscan localised folding to post-Variscan brittle tectonics: structural evolution of the Glinno Graben, Góry Sowie Massif, SW Poland (NE Bohemian Massif)

Aleksander KOWALSKI[1], * and Grzegorz PACANOWSKI[2]

[1] Polish Geological Institute – National Research Institute, Lower Silesia Branch, al. Jaworowa 19, 50–122 Wrocław, Poland; ORCID: 0000-0003-4963-3995

[2] Polish Geological Institute – National Research Institute, Rakowiecka 4, 00–975 Warszawa, Poland; ORCID: 0000-0001-9045-3262

We have combined traditional geological field mapping, LiDAR-based digital elevation model (DEM) analysis, and shallow 2D Electrical Resistivity Tomography (ERT) to investigate the syn- to late-orogenic Mississippian ('*Culm*') succession preserved in the Glinno Graben (NE Bohemian Massif, SW Poland), and to propose a new model for its multistage tectonic evolution. The Glinno Graben, situated in the Góry Sowie Massif (GSM) southwest of the Sudetic Boundary Fault, is ~7.5 km long, up to 1.5 km wide, and has a markedly asymmetrical internal structure. Structural and geophysical data, supported by regional evidence from the nearby Kamionki Graben, suggest that the main boundary faults of the graben originated during a late Carboniferous to early Permian extensional or transtensional phase, following folding of the Mississippian strata, likely during the Namurian. A subsequent compressional episode during the Late Cretaceous to early Paleogene interval reactivated pre-existing faults and produced broad, gentle folds within the Carboniferous graben fill. Although direct structural evidence is sparse due to limited exposure, this event is supported by regional tectonic correlations. The final tectonic phase, possibly of Neogene to Quaternary age, was marked by NE–SW extension and resulted in the development of high-angle normal faults and internal compartmentalization of the graben. This phase also controlled the development of structurally induced landslides and the formation of Ostrzew Hill as a resistant erosional outlier in the southern part of the graben. Despite poor bedrock exposure, ERT and DEM analyses consistently delineated boundary faults and internal segmentation of the graben. This integrated approach provides the first detailed structural characterization of the Glinno Graben atop the GSM and highlights the long-term reactivation of inherited basement discontinuities.

Key words: Variscan folding, Sudety Mts., Mississippian, Alpine inversion, Electrical Resistivity Tomography (ERT), LiDAR DEM analysis.

INTRODUCTION

The Góry Sowie Massif (GSM), a high- to medium-grade metamorphic unit forming part of the Variscan orogenic belt at the NE margin of the Bohemian Massif (e.g., Mazur et al., 2006), is locally overlain by up to 300 m of unmetamorphosed lower Carboniferous continental and marine deposits preserved in isolated grabens and half-grabens (Fig. 1; Oberc, 1949; Żakowa, 1963; Łapot, 1986; Kowalski, 2024; Kowalski and Pacanowski, 2025). These structures are regarded as tectono-erosional vestiges of a formerly more extensive late-Variscan basin system that once developed in southwestern Poland (Narkiewicz, 2007, 2020; Kowalski and Pacanowski, 2025). Despite its limited geographic extent, the Carboniferous succession of the GSM holds significant regional importance, as it preserves a localized record of late Variscan folding during the late Mississippian (possibly extending into the Namurian), followed by the extensional collapse of the Sudetic segment of the Variscan orogen. This was succeeded by a late Carboniferous to early Permian extensional or transtensional tectonic phase (Kowalski and Pacanowski, 2025). The NW–SE-oriented grabens preserved atop the GSM also record a major reorganization of regional stress regimes, marked by Late Cretaceous to early Paleogene compression, followed by a renewed phase of extensional tectonics. These processes are consistent with deformation patterns observed in other tectonic units across the northeastern Bohemian Massif (Oberc, 1972; Solecki, 1994, 2011; Don, 2003; Don and Gotowała, 2008; Coubal et al., 2015; Kowalski, 2021a; Sobczyk and Szczygieł, 2021; Voigt et al., 2021; Głuszyński and Aleksandrowski, 2022; Kowalski and Pacanowski, 2025).

* Corresponding author, e-mail: aleksander.kowalski@pgi.gov.pl

Recent structural and geophysical studies have provided new insights into the relationship between the multiply deformed late Paleozoic sedimentary cover and the metamorphic basement of the GSM, particularly in the area of the Kamionki Graben and its surroundings (Kowalski and Pacanowski, 2025; Kowalski, 2025). The present study continues this line of research by extending the regional framework through a detailed structural and geophysical analysis of its northeastern prolongation, the Glinno Graben (GG), a distinct tectonic trough situated adjacent to the previously investigated area.

This contribution incorporates new geological mapping and geophysical data to reassess the tectonic framework originally proposed in classic studies (Dathe and Finckh, 1924; Oberc, 1949, 1972; Teisseyre and Sawicki, 1958; Żakowa, 1960; Grocholski, 1962, 1965). The GG has previously been the subject of geological mapping at 1:25,000 scale (Dathe and Finckh, 1924; Teisseyre and Sawicki, 1958; Grocholski, 1962), along with biostratigraphic (Żakowa, 1959, 1960) and petrographic investigations (Łapot, 1986, 1988). More recently, structurally-controlled landslides have been reported in the southern sector of the GG, together with a proposed reinterpretation of the geological structure of this part of the graben (Kowalski, 2018). Nevertheless, the internal structure of the GG remains poorly understood.

To address this gap, we integrated traditional geological field mapping with high-resolution LiDAR-derived digital elevation models (DEMs) and shallow two-dimensional Electrical Resistivity Tomography (ERT) surveys. In the absence of borehole data, 2D ERT proved especially effective in delineating the geometry of the Mississippian graben-fill and the configuration of its bounding faults. This integrated structural-geophysical approach refines our understanding of the tectonic evolution of the GSM and provides new insights into the deformation styles of the early Carboniferous succession during late- to post-Variscan times on the northeastern Bohemian Massif. In addition, this study offers a broader regional and temporal context for the deformation phases affecting the Mississippian sedimentary cover of the study area.

GEOLOGICAL SETTING

GEOLOGICAL FRAMEWORK OF THE GÓRY SOWIE MASSIF AND ADJACENT UNITS

The GSM, located at the northeastern margin of the Bohemian Massif, forms a fault-bounded, high- to medium-grade metamorphic complex with a roughly triangular surface outline (Fig. 1; Grocholski, 1967; Żelaźniewicz, 1987, 1990; Cymerman, 1998). It marks the northeastern termination of the European Variscides – a vast orogenic belt formed during the late Paleozoic through the collision of Gondwana, the Laurussian supercontinent, and several intervening microcontinents (terranes; e.g., Mazur et al., 2006; Franke et al., 2017; Edel et al., 2018; Martínez-Catalán et al., 2021; Schulmann et al., 2022; Franke and Żelaźniewicz, 2023). Today, this belt extends from the Iberian Peninsula across Central Europe and ultimately plunges beneath the Miocene Carpathian Foreland Basin. The GSM consists predominantly of a monotonous sequence of migmatites, migmatitic paragneisses, and orthogneisses, along with subordinate lens-shaped bodies of amphibolite, ultrabasic rock, crystalline dolomite, and felsic granulite (Grocholski, 1967; Żelaźniewicz, 1987, 1990; Cymerman, 1988, 1989; Gunia, 1999; Jastrzębski et al., 2021, 2025; Tabaud et al., 2021). The paragneisses are interpreted as metamorphosed flysch-like greywackes and pelitic-psammitic deposits of Neoproterozoic to Cambrian age (Żelaźniewicz, 1987; Tabaud et al., 2021) supported by the presence of microfossils (Gunia, 1999). U-Pb zircon data further suggests a peri-Gondwanan provenance for these deposits (Tabaud et al., 2021; Jastrzębski et al., 2025). Protoliths of the metaigneous rocks, now mainly orthogneisses of crustal origin, have been dated to ~500–490 Myr (Kröner and Hegner, 1998; Kryza and Fanning, 2007). The protoliths of gneisses and migmatites of the GSM were metamorphosed under amphibolite facies conditions during the early Late Devonian (~380–370 Ma; Van Breemen et al., 1988). An earlier episode of high-pressure, high-temperature (HP–HT) metamorphism in granulites and associated metaperidotites took place at ~400–395 Ma and was subsequently overprinted by amphibolite-facies retrogression (Kryza and Fanning, 2007). This metamorphic evolution was followed by rapid uplift and exhumation of the GSM during the Late Devonian (Żelaźniewicz, 1987; Bröcker et al., 1998), a process recorded in the sedimentary infill of surrounding basins such as the Świebodzice and Bardo units (Wajsprych, 1978; Porębski, 1981; Haydukiewicz, 1990). Together with the Kłodzko Metamorphic Unit, the GSM is interpreted as a relict of the allochthonous Teplá–Barrandia–Bohemia terrane, part of the Eo-Variscan domain near Gondwana's northern margin during the Cambrian–Ordovician (Mazur et al., 2015; Martínez-Catalán et al., 2021; Jastrzębski et al., 2021, 2025; Tabaud et al., 2021; Franke and Żelaźniewicz, 2023).

The GSM is dissected by the NW–SE-trending Sudetic Boundary Fault, which separates the massif into two mutually displaced segments: the mountainous, upthrown block to the SW (Sudetic Block) and the downthrown block to the NE (Fore-Sudetic Block; Fig. 1; Oberc and Dyjor, 1969; Badura et al., 2007; Migoń et al., 2023). Geophysical data indicate that the structural levels exposed in the Fore-Sudetic Block are ~5 km deeper than those in the Sudetic part of the massif (Oberc, 1972; Cwojdziński and Żelaźniewicz, 1995). The absence of Carboniferous (and younger) strata in the Fore-Sudetic Block is likely due to post-Carboniferous erosion (Oberc, 1972), although it cannot be excluded that this area acted as a topographically elevated source region where sediments never accumulated. To the west, the GSM is bordered by the Głuszyca Fault, separating it from the Intra-Sudetic Basin – a synclinorial unit containing a weakly deformed Mississippian to Upper Cretaceous volcano-sedimentary succession (Augustyniak and Grocholski, 1968; Nemec et al., 1982; Dziedzic and Teisseyre, 1990; Wojewoda, 1997; Kowalski, 2020, 2021b). The northern edge of the GSM is tectonically bounded by the Świebodzice Unit, a syn-orogenic Upper Devonian–Mississippian sedimentary succession (Porębski, 1981, 1990), while to the south, Devonian–Mississippian clastics and carbonates of the Bardo Unit – including older olistoliths – are exposed (Wajsprych, 1978; Haydukiewicz, 1990; Racki et al., 2022). Complexes of mafic to ultramafic rocks, surrounding the GSM, belong to the dismembered Central Sudetic Ophiolite (~400 Myr), including the Ślęża, Szklary, Braszowice, and Nowa Ruda massifs (Dubińska and Gunia, 1997; Awdankiewicz et al., 2021; Wojtulek et al., 2022). Notably, ophiolites of the Nowa Ruda Massif are overlain by Pennsylvanian clastic deposits within the eastern Intra-Sudetic Basin (Bossowski and Ihnatowicz, 2006). To the east, the GSM is flanked by the NNE–SSW-striking Niemcza Shear Zone, a polygenetic zone of mylonitized gneisses intruded by small granitic bodies (Mazur and Puziewicz, 1995; Pietranik et al., 2013), which separates the massif from the Kamieniec Metamorphic Belt.
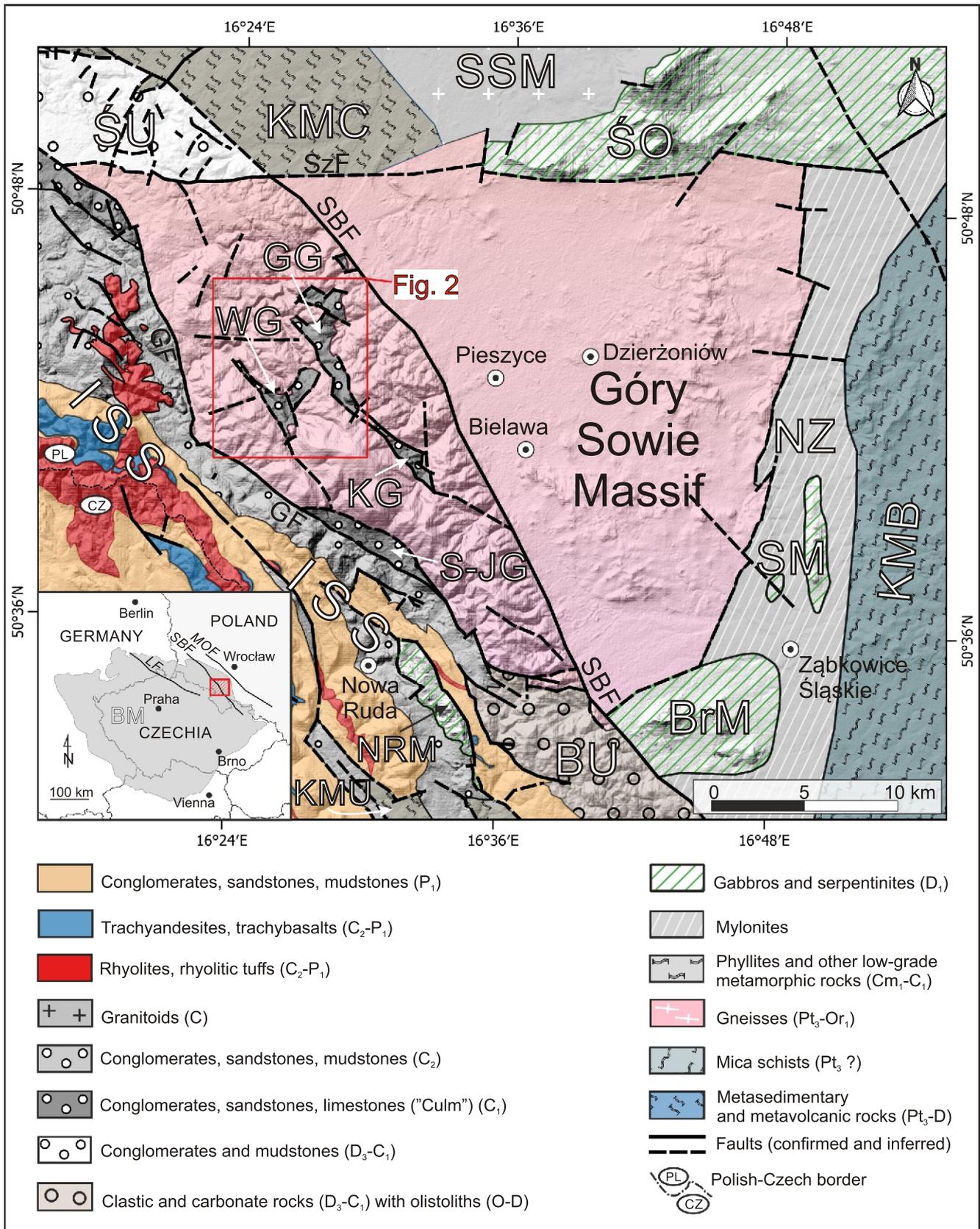
Fig. 1. Simplified tectonic map of the Góry Sowie Massif and neighbouring units, with their location in the NE Bohemian Massif (inset). The map is overlaid onto the digital elevation model (DEM) derived from the Shuttle Radar Topography Mission (SRTM) data (NASA, 2001; Farr et al., 2007)

BrM – Braszowice Ophiolite Massif, BU – Bardo Unit, GG – Glinno Graben, ISS – Intra-Sudetic Synclinorium, KG – Kamionki Graben, KMB – Kamieniec Metamorphic Belt, KMC – Kaczawa Metamorphic Complex, KMU – Kłodzko Metamorphic Unit, NRM – Nowa Ruda Ophiolite Massif, NZ – Niemcza Shear Zone, S-JG – Sokolec-Jugów Graben, SM – Szklary Ophiolite Massif, SSM – Strzegom-Sobótka Granitoid Massif, ŚO – Ślęża Ophiolite Massif, ŚU – Świebodzice Unit, WG – Walim Graben. Faults: GF – Głuszyca Fault, MOF – Middle Odra Fault, LF – Lusatian Fault, SBF – Sudetic Boundary Fault, SzF – Szczawienko Fault. Geological map based on Sawicki (1995), modified and supplemented by the authors

THE GLINNO GRABEN AS PART OF THE CARBONIFEROUS SEDIMENTARY COVER OF THE GÓRY SOWIE MASSIF

Remnants of a middle Viséan to Namurian(?) Mississippian sedimentary succession are preserved exclusively in the elevated Góry Sowie Mountains Block, south-west of the Sudetic Boundary Fault (Fig. 1). Traditionally known as the "*Culm of the Sowie Mountains*" (Żakowa, 1963; Oberc, 1972; Łapot, 1986, 1988), these deposits are restricted to several small, NW–SE-trending fault-bounded grabens and half-grabens, including the Walim, Glinno, Kamionki, and Sokolec–Jugów grabens (Fig. 1). The preserved strata reach up to 300 m in thickness and are subdivided into three distinct lithostratigraphic units (Kowalski, 2024).

The lowest unit comprises poorly sorted "gneissic" and "gabbroic" conglomerates and sedimentary breccias (Fig. 2), classified as the Walim and Jugów formations, which rest unconformably on the metamorphic GSM basement (Łapot, 1986). The gneissic conglomerates of the Walim Formation occupy the largest area within the Glinno Graben and are interpreted as alluvial fan deposits formed along tectonically active basin margins (Kowalski, 2024, 2025). These grade upwards into lithic (gneissic) sandstones, followed by marine sandstones and mudstones of the Sokolec Formation, up to 100 m in thickness. Gneissic conglomerates and sandstones in the northern GG are intruded by small kersantite sills (Żakowa, 1960; Awdankiewicz, 2007). Initially assigned to the upper Viséan based on macrofaunal assemblages (Żakowa, 1959, 1960, 1963, 1966; Żakowa and Żak, 1962), the upper part of the Sokolec Formation may extend into the Namurian(?) (Muszer et al., 2016; Górecka-Nowak et al., 2025). Notably, the Sokolec Formation is only preserved as an erosional outlier on Ostrzew Hill at the southern end of the GG, where it is intruded by a tabular (sheet-like) kersantite body with an estimated thickness of ~35 m (Łapot, 1986; Kowalski, 2018). The uppermost unit, the Kamionki Formation, consists of ~80 m of Namurian(?) polymictic conglomerates, well exposed in the Kamionki and Sokolec–Jugów grabens (Żakowa and Żak, 1962; Żakowa, 1966; Kowalski and Pacanowski, 2025; Kowalski, 2025). These deposits are interpreted as fan deltas that prograded into the Carboniferous basin from the north and northwest (Kowalski, 2024, 2025). This formation is absent from the GG, likely due to post-Carboniferous erosion.

The tectonic setting of the GG has remained poorly understood to date, largely due to the absence of borehole data and limited geophysical imaging. The basal Carboniferous unconformity has been penetrated by hydrogeological boreholes only in the adjacent Kamionki Graben, at depths of 110 and 143 m (SPDPSH, 2025; Kowalski and Pacanowski, 2025). Consequently, the magnitude of vertical displacement along the main boundary faults of the grabens remains unresolved. Dathe and Finckh (1924), followed by Teisseyre and Sawicki (1958), originally assumed that the northern part of the GG was bounded by relatively simple, steeply dipping vertical faults. In contrast, Oberc (1972) offered a more complex interpretation, describing the GG as a "*secondarily disturbed syncline*" composed of fault-bounded Carboniferous rocks. Within this framework, Oberc (1972) identified three subordinate structural units – interpreted as separate, minor grabens – arranged from north to south: the Przygrodna Graben, the Cerekwica Graben (or "*the system of Cerekwica grabens*"), and the Glinno Graben.

MATERIAL AND METHODS

This study is based on new geological mapping, LiDAR-derived DEM analysis, and structural investigations, complemented by two-dimensional Electrical Resistivity Tomography (ERT). These methods were integrated to reconstruct the geometry and tectonic evolution of the GG.

MAPPING SURVEY AND STRUCTURAL FIELD STUDY

The geological field survey covered ~8 km² and was supported by analysis of high-resolution LiDAR-derived digital elevation models (DEMs) at ~1 x 1 m resolution. The elevation data were acquired through airborne laser scanning (ALS) conducted in Poland between 2011 and 2014 under the ISOK program (IT System for the Country's Protection against Extreme Hazards). The data, provided by the Polish Centre of Geodetic and Cartographic Documentation (CODGiK), are openly available as XYZ point datasets, with a point density of 4–6 points/m² and an average vertical accuracy of ±0.3 m (Wężyk, 2015). Shaded relief maps derived from these DEMs proved invaluable for identifying lithological boundaries and surface fault traces, which were interpreted using *GIS* software. The elevation models also facilitated interpretation of tectonically influenced morphological features such as lineaments linked to suspected faults and rectilinear zones marking lithological changes. The surface extent of the Carboniferous deposits in the GG was corroborated through trenching and shallow drilling conducted during surface geological mapping (Cymerman et al., 2023). In addition to geological mapping, seven ERT cross-sections with a total length of 5140 m from the central and southern parts of the GG were used to construct interpretative geological profiles across the graben structure (Table 1).

The structural field study focused on detailed measurements from both natural and artificial exposures within the graben. Observations were conducted in nine available exposures. Structural features recorded included bedding planes, joints, striated fault planes and folds. Fracture data were classified into sets and visualized using circular frequency polygon plots following Davis and Sampson (1986). Surface features observed on fault planes include striated ridges, hackles, grooves, Riedel shears (both low- and high-angle), and en echelon tension cracks, following the classification and terminology established by Petit (1987). Structural measurements were plotted on   and   stereograms using the lower hemisphere equal-area Schmidt–Lambert net.

GEOPHYSICAL SURVEY

Two-dimensional Electrical Resistivity Tomography (ERT) was employed to visualize the subsurface structure and delineate the main boundary faults of the GG. A total of seven ERT profiles, with a total length of 5140 m, were acquired across the study area (Ostrowski et al., 2022; Table 1). The geophysical profiles were established roughly perpendicular to the map-view elongation of the GG and its fault boundaries, limited by technical feasibility and field conditions. The methodology applied enabled the identification of the position and lateral extent of the graben infill, major lithological boundaries within the GG, and the characterization of suspected faults and fault zones – features that had also been recognized through detailed field mapping and LiDAR-based DEM analysis.

For each lithological unit identified along the ERT profiles, statistical parameters describing the distribution of resistivity values were calculated to characterize the geoelectrical properties of the lithologies distinguished. The analysis included the minimum and maximum resistivity values, as well as the geometric mean and median, expressed both in m and as base-10 logarithms ($\log_{10}$ [m]; Table 1). These parameters were extracted from discrete zones delineated within the two-dimensional inversion models, representing relatively homogeneous resistivity intervals associated with specific lithological units. The geometric mean was used to describe the central tendency of resistivity values, as such data in multiscale porous media typically follow a log-normal distribution (Kurochkina et al., 2008; Binley and Slater, 2020). Lithological classification
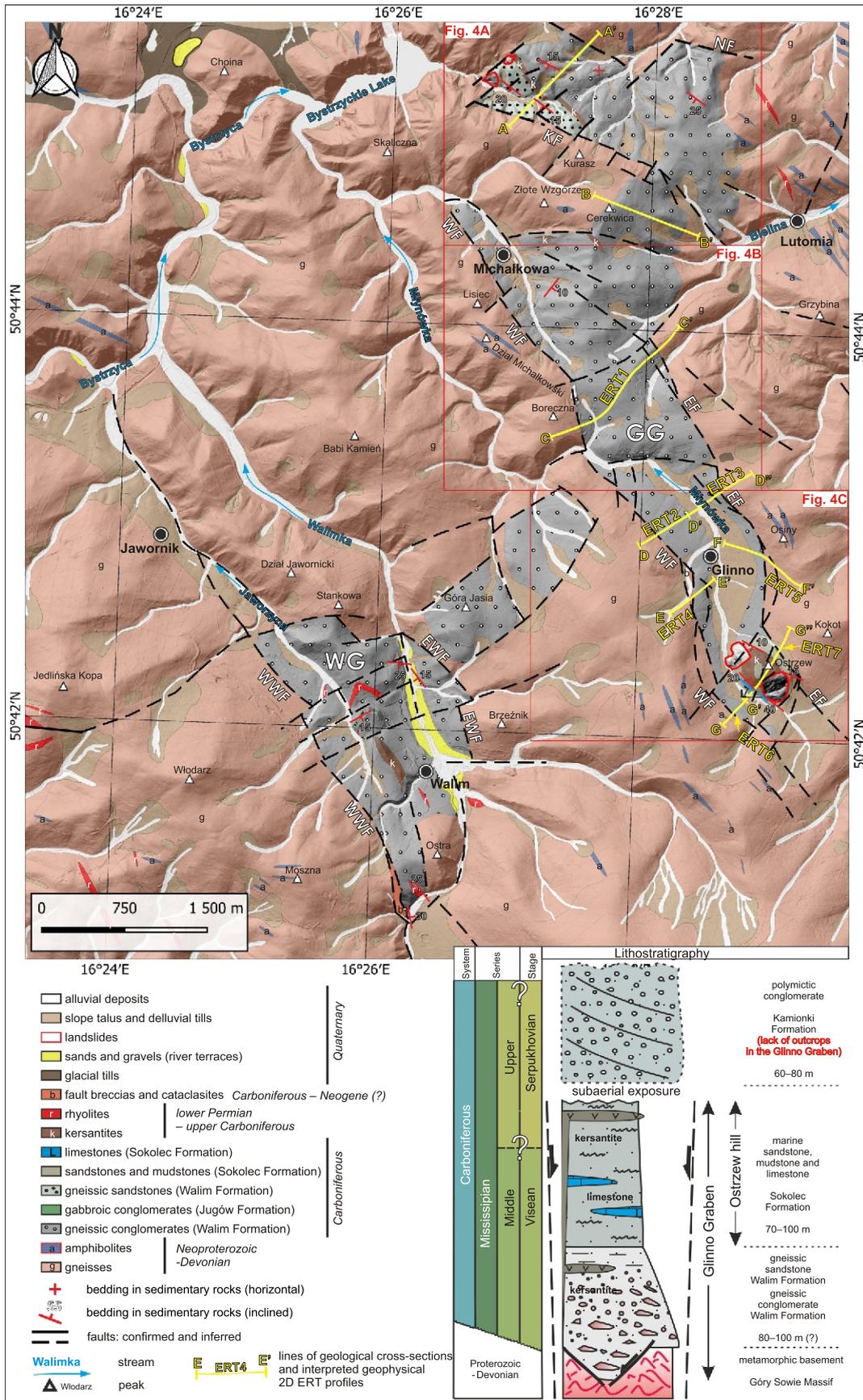
Fig. 2. Geological map of the Glinno (GG) and Walim (WG) grabens (for location see Fig. 1), including a synthetic lithostratigraphic scheme of the Carboniferous succession preserved in the Glinno Graben

The locations of geological cross-sections shown in Figure 6 and ERT profiles from Figures. 8 and 9 are marked. The main exposures referred to in the text are also indicated. The extent of unconsolidated Quaternary deposits is shown courtesy of Joanna Brytan (PGI-NRI). Basement geology simplified after Teisseyre and Sawicki (1958) and Grocholski (1967); geology of the Mississippian graben fill based on the author's own geological mapping conducted as part of this study. Abbreviations: GG – Glinno Graben, EF – Eastern Glinno Fault, KF – Kurasz Fault, NF – Northern Glinno Fault, WG – Walim Graben, WF – Western Glinno Fault. Red rectangles indicate the extent of the detailed geological maps shown in Figure 4

T a b l e 1

Summary of ERT profiles acquired in the Glinno Graben area

Profile	Length [m]	Orientation (course)	Number of measured points	Mean RMS error [%]
ERT-1	1550	SW-NE	7867	2.17
ERT-2	600	SW-NE	1613	2.80
ERT-3	600	SW-NE	1678	4.12
ERT-4	500	SW-NE	1258	2.50
ERT-5	800	NW-SE	2357	3.20
ERT-6	300	SW-NE	597	2.94
ERT-7	790	SW-NE	2388	4.74

The table includes basic parameters of each Electrical Resistivity Tomography (ERT) profile: name, total length [m], location and orientation, number of measured points, and average root mean square (RMS) error [%] from the inversion process

within the ERT sections was performed based on assumed resistivity intervals, a standard approach in geophysical interpretation grounded in previous studies and reference datasets (Reynolds, 2011). This approach enabled quantitative comparison across different lithologies and provided additional constraints for geological interpretation and correlation.

Prior to the geophysical survey, each survey point was accurately geolocated using differential-phase GNSS methods, achieving a horizontal positioning precision of ~0.3 m. Coordinates were assigned within the PL-1992 spatial reference system. The quality of the satellite data allowed full use of GNSS-based geodesy across the entire profile network. Elevation values for the documentation points were established through RTN (Real-Time Kinematic) satellite levelling and referenced to the national vertical datum PL-EVRF2007-NH.

2D ELECTRICAL RESISTIVITY TOMOGRAPHY

Electrical resistivity methods rely on measuring an artificially induced electric field within the geological medium or, less commonly, on detecting natural electric currents and fields generated by geodynamic or geochemical processes in the Earth's crust. The key physical parameter obtained through these methods is electrical resistivity, which quantifies a material's capacity to resist the flow of electric current (Reynolds, 2011). Resistivity values can vary by several orders of magnitude, from a few Ωm in organic-rich deposits or saline groundwater, to several million Ωm in dry crystalline bedrock. Unlike properties such as density or magnetic susceptibility, electrical resistivity is not a fixed material constant, but rather a function of multiple interrelated factors. These include lithology, porosity, degree of water saturation, temperature, pore water chemistry, and the presence of organic matter or gas. As a result, even within a single lithological unit, resistivity may exhibit substantial internal variation.

Electrical Resistivity Tomography (ERT) is a near-surface geophysical technique that measures the apparent resistivity of subsurface materials by injecting direct current between electrode pairs and recording the resulting voltage drop. The theoretical basis of the ERT method has been well established in foundational works (Keller and Frischknecht, 1966; Loke and Barker, 1996; Dahlin and Zhou, 2004; Loke, 2000, 2012). The method involves deploying electrodes along a linear profile, injecting current through a transmitter electrode pair, and measuring the voltage drop between a separate pair of potential electrodes. The resulting apparent resistivity is an averaged value dependent on the geometry of the electrode array and reflects the properties of the subsurface volume traversed by the

current. The depth of investigation primarily depends on the electrode spacing, the resistivity distribution and, to a lesser extent, local topography.

Modern ERT systems use computer-controlled multi-channel switching and digital acquisition units. These allow for automated configuration of electrode arrays (e.g., Wenner, Schlumberger, dipole–dipole, gradient), sequencing of measurements, and real-time diagnostics of grounding resistance and data quality. Inversion algorithms are used to generate two-dimensional resistivity models from apparent resistivity datasets, commonly corrected for topography. ERT enables the detection of both vertical and lateral resistivity variations, making it particularly suitable for structurally complex settings such as glaciotectonic zones (Loke et al., 2007). However, inversion results are inherently non-unique, meaning that multiple subsurface models can explain the same data equally well (Bania et al., 2024).

In this study, data were acquired using an ABEM Terrameter LS 2 system equipped with a multi-channel module and an automatic electrode selector (ABEM, 2012; Ostrowski et al., 2022). Electrodes were spaced at 5 m intervals and connected via 21-takeout multicore cables (Fig. 3). Survey lines ranged from 300 to 1550 m in length. A gradient array was used to enable multiple simultaneous measurements, improving data acquisition efficiency and ensuring that depth penetration exceeded 50 m. The Roll-Along technique was applied in the field, whereby the first cable section was relocated to the front of the array, allowing continuous profiling without full system reconfiguration. Survey conditions were locally constrained by infrastructure, including an asphalt road that intersected one of the profiles (Pacanowski et al., 2022). Resistivity measurement data were processed using geophysical inversion techniques implemented in *Res2Dinv* software (Loke, 2000), version x64 4.02.35. The inversion employed the L1-norm (robust) method, optimized for resolving blocky subsurface structures.

ERT techniques have been widely applied in geological, geomorphological, hydrogeological, geotechnical and environmental investigations (e.g., Zhou et al., 2001, 2002; Kemna et al., 2002; Chambers et al., 2006; Krautblatter and Hauck, 2007; Ostrowski et al., 2010; Šilhán and Pánek, 2010; Putiška et al., 2012; Perrone et al., 2014; Kowalczyk et al., 2015; Topolewska et al., 2016; Woźniak et al., 2018; Ducut et al., 2022). 2D ERT has been also widely applied for fault characterization and imaging of individual fault zones (e.g., Suzuki et al., 2000; Caputo et al., 2003; Zhu et al., 2009; Štěpančíková et al., 2010, 2011, 2025; Fischer et al., 2012; Imposa et al., 2015; Drahor and Berge, 2017; Mojica et al., 2017; Müller et al., 2020; Porras et al., 2022).
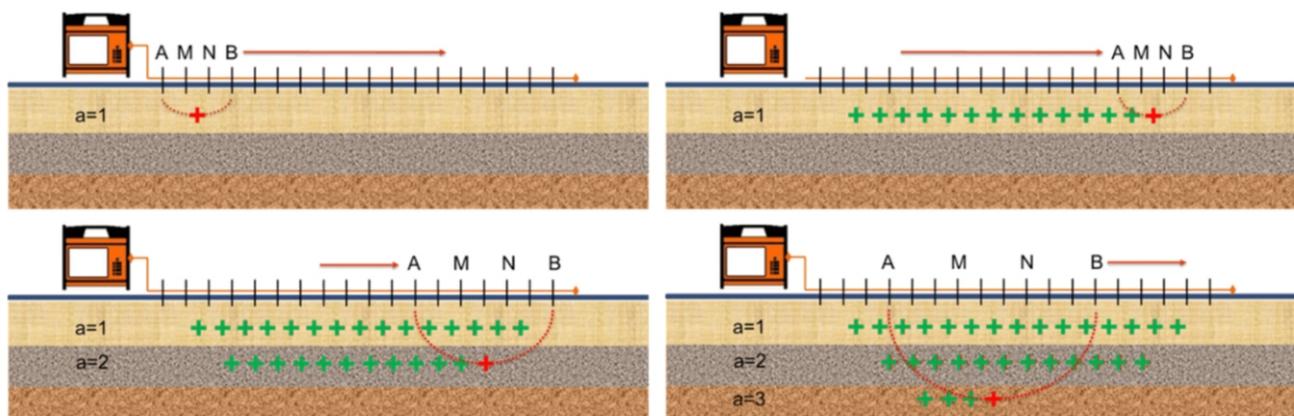
Fig. 3. Graphical representation of the automated data acquisition procedure performed by the instrument (source: https://www.guidelinegeo.com)

A, B – current electrodes; M, N – potential electrodes; a=1, a=2, a=3 – successive prospection depths

RESULTS

GEOLOGICAL MAPPING

On the map, the GG appears as an ~7.5 km-long and up to 1.5 km-wide, asymmetrical fault-bounded tectonic depression (Figs. 2 and 4). It comprises at least three distinct tectonic sub-units, each delineated by the main boundary faults of the graben and by subordinate fault zones (Fig. 4). The graben is developed atop the crystalline basement of the GSM, primarily composed of migmatitic and biotite paragneisses with minor amphibolite bodies (Teisseyre and Sawicki, 1958; Grocholski, 1962). The main boundary faults of the graben – here referred to as the Western, Eastern, Northern Glinno, and Kurasz faults (Fig. 4) – separate the Mississippian graben fill from the surrounding metamorphic basement (Fig. 4). However, the vertical and possible horizontal displacements along these faults remain unconstrained due to limitations in surface exposure and the absence of borehole data. Moreover, none of the 2D ERT profiles conducted in this study reached the metamorphic basement beneath the graben, further limiting our ability to determine the total thickness of the sedimentary infill and the displacement values along the fault zones.

The northernmost sector of the GG (the Przygrodna Graben of Oberc, 1972) displays a WNW–ESE-striking half-graben structure, predominantly filled with gneissic conglomerates and sandstones of the Walim Formation (Figs. 4A and 5). The conglomerates are clast- to matrix-supported and are predominantly very poorly sorted (Fig. 5A–C). Large clasts and boulders found at the surface, particularly in the northern part of the GG, are derived from the weathering of conglomerates (Fig. 5D, E). The clasts, which show variable degree of rounding, include migmatitic gneisses, biotite-oligoclase paragneisses, fibrous gneisses, granulites, orthogneisses, fragments of other metamorphic rocks, and vein quartz (Łapot, 1986, 1988; Fig. 5F). The gneissic clasts within the conglomerate are frequently fractured, displaying both macro- and microfractures, with fracture surfaces commonly coated with hematite. The grain framework is filled by a sandstone matrix composed of clastic material derived from the disintegration of gneissic rock fragments. These strata generally dip gently at 15–20° to the south-west and are intersected by narrow, WNW–ESE-trending lamprophyre dykes (Figs. 4A and 6). In the northern part of the GG, the gneissic conglomerates locally rest horizontally, which may suggest the presence of a flexure (Fig. 4A and 6). Additionally, this part of the graben is dissected by several NNE–SSW-oriented transverse faults, which locally offset the Mississippian succession and its basement – particularly on the northern slopes of Kurasz Hill – and contribute to its structural compartmentalization. Some of these dislocations are clearly expressed in the landscape as distinct scarps and lineaments (Fig. 4A). Notably, in the easternmost part of this part of the GG, the gneissic conglomerates rest nearly horizontally on the metamorphic basement, with no clear evidence of bounding faults.

To the south, the half-graben merges with a NNE–SSW-oriented fault-bounded gneissic block (the Cerekwica Graben of Oberc, 1972), overlain by a thin carpet of gneissic conglomerates near Cerekwica Hill (Figs. 4A and 6). This block is separated from the northern part of the graben by the WNW–ESE-trending Kurasz Fault. The central portion of the GG forms a distinct topographic depression (the main body of the GG), aligned with the Młynówka stream valley and extending between the villages of Michałkowa and Glinno (Figs. 4B, C and 6). It is bounded by two nearly parallel, NW–SE-trending boundary faults (the Western and Eastern Glinno faults), with total trace lengths of ~6.5 km and 4 km, respectively. This sector exposes only gneissic conglomerates of the Walim Formation (Figs. 4A, 5C and 6). To the south of Boreczna Hill, the GG is separated from the neighbouring Walim Graben by a narrow NW–SE-trending basement horst (Figs. 2 and 4B). Geological mapping revealed a prominent cataclasite zone up to 70 m wide, aligned along the Western Glinno Fault (Fig. 4C). This zone consists of fault gouges and breccias, with angular fragments of gneiss at the contact between the gneissic conglomerates and crystalline basement.

In the southernmost part of the GG, a morphological high known as Ostrzew Hill (713.4 m a.s.l.) rises ~150 m above the graben floor (Figs. 4C, 6 and 7). This erosional outlier exposes sandstones and mudstones of the Sokolec Formation, intruded in its upper part by a tabular kersantite body, while gneissic conglomerates of the Walim Formation crop out on the lower slopes (Figs. 4C, 6 and 7). The structure of this sector is well constrained based on surface exposures and archival trenching data, including studies by Żakowa (1959, 1960). Sandstones and mudstones of the Sokolec Formation, form a broad, NW–SE-oriented syncline, with its axial trace aligned with the
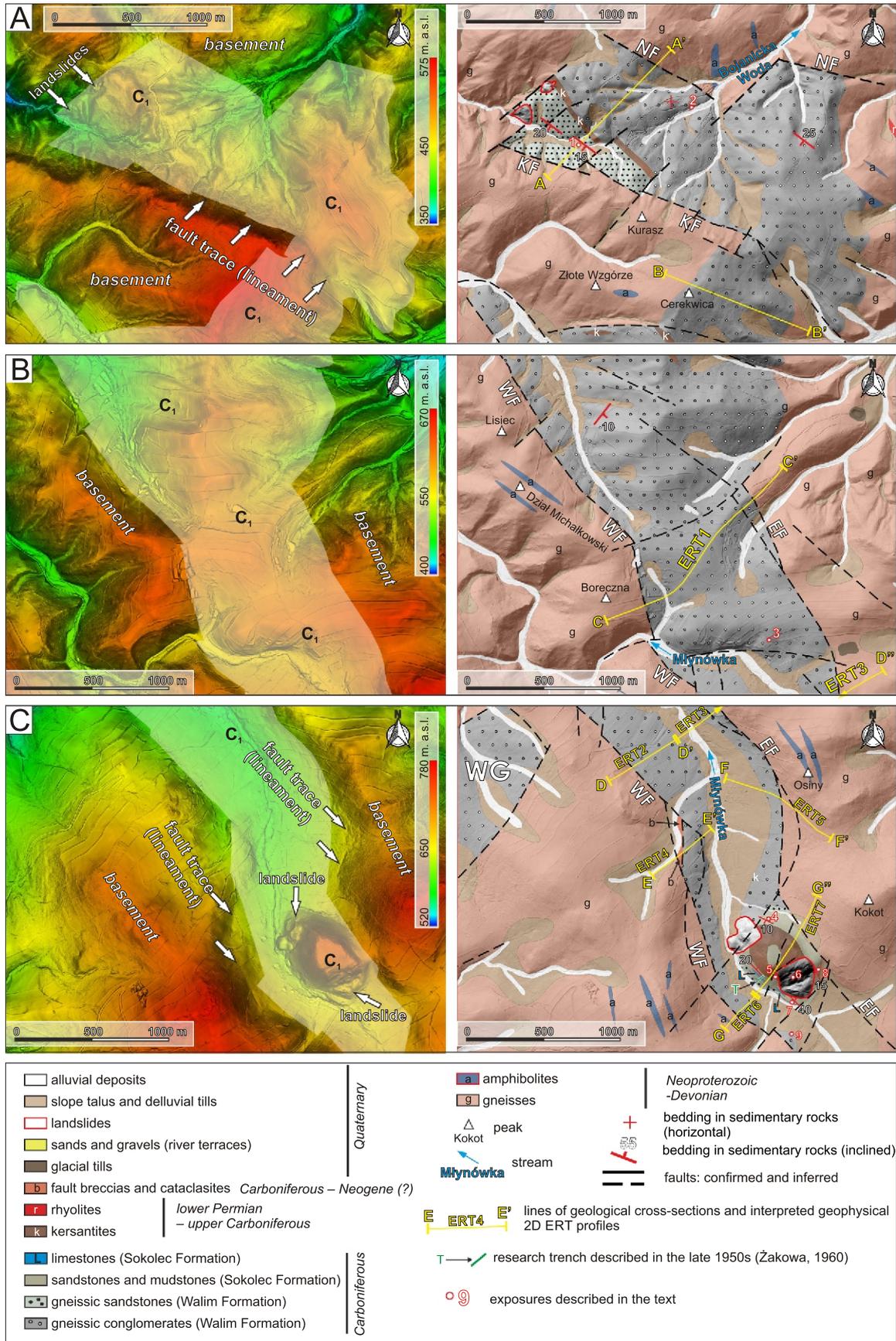
Fig. 4. Detailed geological maps showing the northern (A), central (B), and southern (C) sectors of the Glinno Graben, along with corresponding hillshaded LiDAR-derived digital elevation models (shown to the left of each map panel). Note the presence of distinct lineaments (marked fault traces) through the graben area and structurally controlled landslides in its southernmost sector (C)
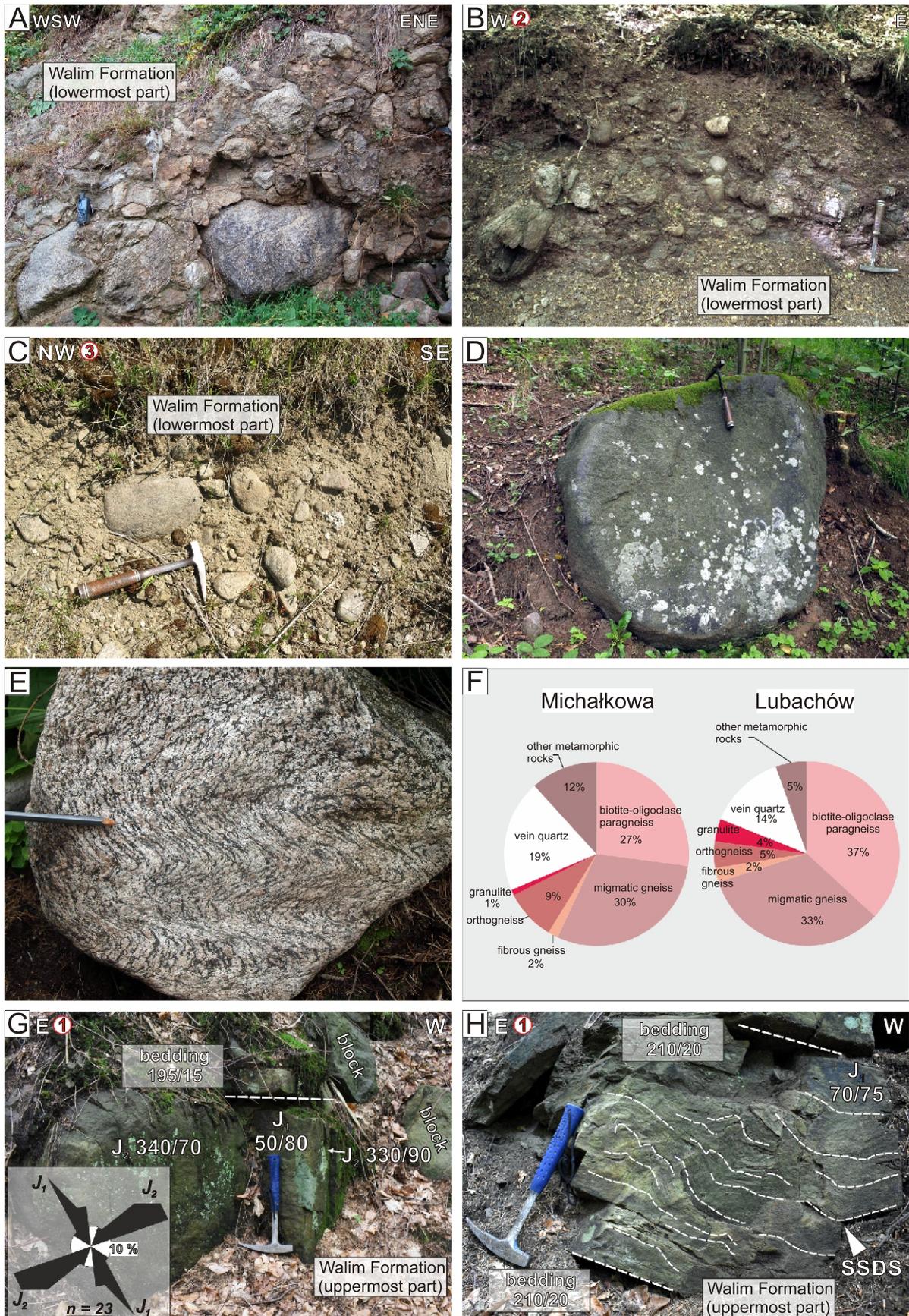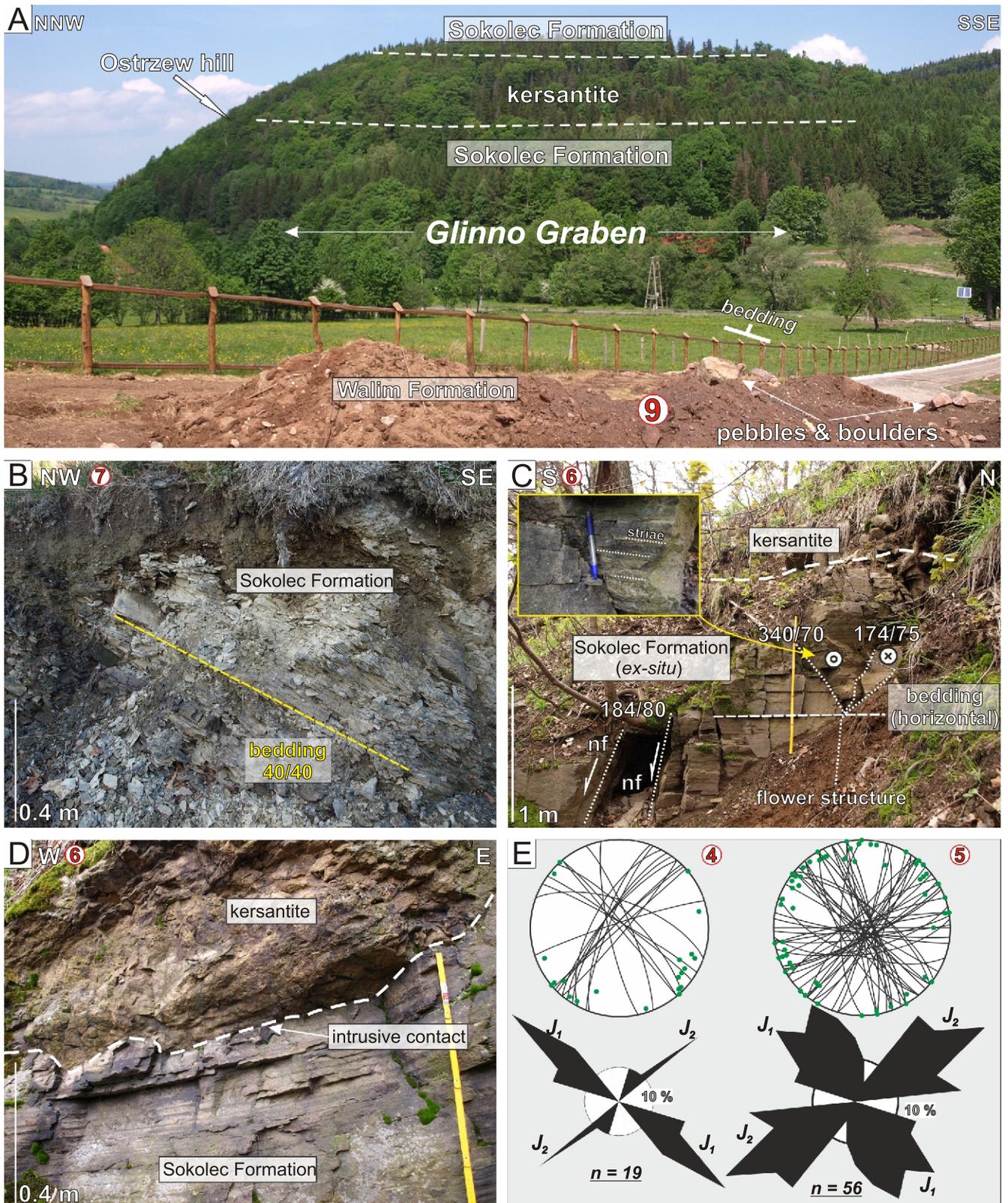
Fig. 5. Main lithological and structural features of the Walim Formation in the study area and its surroundings

A – representative exposure of gneissic conglomerate in the adjacent Walim Graben; **B** – exposure of gneissic conglomerate (loc. 2) in the northern part of the GG; **C** – exposure of gneissic conglomerate (loc. 3) in the central part of the GG; **D** – well-rounded boulder derived from the weathering of gneissic conglomerate (northern sector of the GG); **E** – clast of folded and migmatized layered gneiss from the gneissic conglomerate (northern sector of the GG); **F** – petrographic composition of clasts in the conglomerates of the Walim Formation at Michałkowa (central part of the graben) and Lubachów (northern part), after Łapot (1986); **G** – joint system in gneissic sandstone in the northern part of the GG (loc. 1). Orientation of joints is shown as a rose diagram (circular frequency polygon plot); **H** – small-scale, S- to SW-vergent folds in a limited exposure of Walim Formation sandstones (loc. 1). The folds are interpreted as a soft-sediment deformation structure (SSDS)
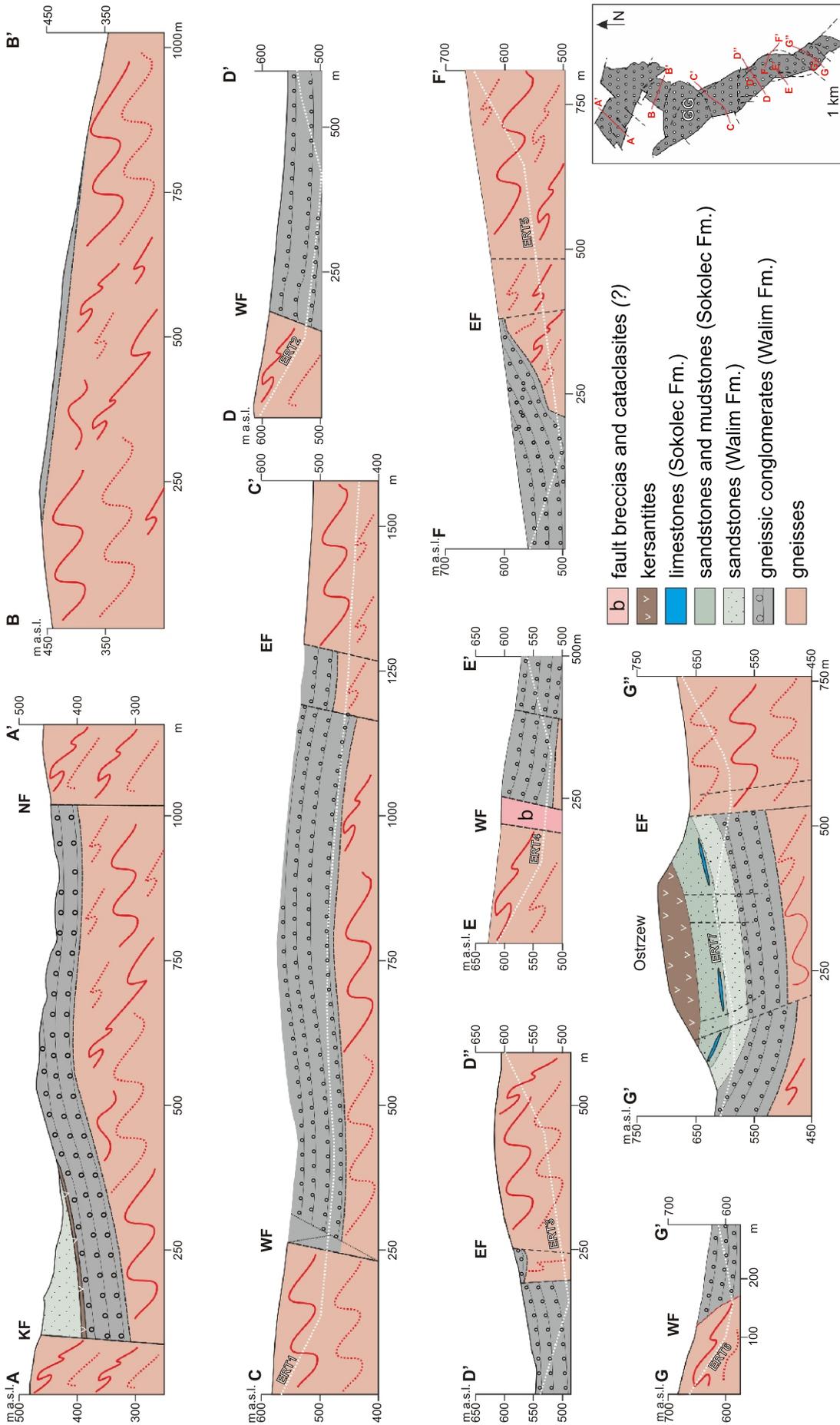
Fig. 6. Geological cross-sections across the Glinno Graben based on mapping field traverses and geophysical profiles shown in Figures 8 and 9

See inset map in the lower right corner and Figure 4 for location of the cross-sections. Explanations of abbreviations (faults) as in Figures 2 and 4. The depth range of corresponding ERT profile is indicated on each section

Fig. 7. Main lithological and structural features of the Sokolec Formation in the Glinno Graben

A – view from the southwest (loc. 9) towards the Ostrzew Hill outlier located in the axial part of the Glinno Graben. The reddish weathering cover of gneissic conglomerates of the Walim Formation is visible; **B** – exposure of fine-grained sandstones and mudstones of the Sokolec Formation (loc. 7) in the southern part of the GG (southwestern slopes of Ostrzew Hill); **C** – exposure of sandstones (loc. 6) within a landslide block on the southern slope of Ostrzew Hill. Contact with a kersantite intrusion is visible. Strike-slip fault of undetermined slip sense forming a negative flower structure, and associated E–W-trending normal faults are observed; **D** – intrusive contact between sandstones of the Sokolec Formation and kersantite at loc. 6 (landslide body in southern Ostrzew Hill); **E** – two dominant joint sets (J_1 and J_2) cutting sandstones (loc. 4) and kersantites (loc. 5) in the southern part of the GG. Orientation of joints is shown as rose diagrams (circular frequency polygon plots) and as stereoplots (the lower hemisphere, equal area projections on the Schmidt-Lambert net)

graben's general trend (Figs. 4C and 6). This part of the GG also includes two structurally controlled landslides developed on the northwestern and southern slopes of Ostrzew Hill (Kowalski, 2018). The Western and Eastern Glinno fault zones extend southeastwards into the metamorphic basement of the GSM (Figs. 2 and 4C). Some parts of these fault zones are manifested by distinct straight escarpments (lineaments), along with arrays of water springs and peat bogs (Fig. 4C). Importantly, the uppermost member of the Carboniferous succession preserved in grabens within the GSM – the Kamionki Formation conglomerate – is not exposed anywhere in the GG, likely due to post-Carboniferous erosion.

GEOPHYSICAL SURVEY

Seven geoelectrical profiles, shown as calculated resistivity models (ERT; Figs. 8 and 9), form the primary dataset of the geophysical survey conducted in the GG and serve as the basis for subsequent geological interpretation (Fig. 6). Geological cross-sections, developed by integrating surface mapping with ERT data, constrain the internal geometry and fault architecture of the graben, and clarify the spatial relationship between the Mississippian sedimentary infill and the underlying crystalline basement (Fig. 6). The ERT cross-sections reveal pronounced vertical and lateral variations in resistivity, corresponding to contrasting lithologies: crystalline basement rocks exposed in the graben shoulders and sedimentary fill. These units are clearly separated by well-defined faults or fault zones.

Average resistivity values derived from profiles 1 to 7 offer diagnostic insights into the lithological differentiation of the study area. Based on the statistical analysis of ERT data, Mississippian rocks in the GG – primarily gneissic conglomerates of the Walim Formation – show geometric mean resistivity values ranging from 212.9 to 431.4 m and median values between 205.4 and 441.9 m (profiles ERT-1–ERT-6; Figs. 8 and 9). In contrast, profile ERT-7, which includes both conglomerates and interbedded sandstones of the Sokolec Formation, is characterized by lower resistivity values, with a geometric mean of 140.5 m and a median of 148.8 m (Table 2). The shallow resistivity inhomogeneities visible in profiles 1–6 (Figs. 8 and 9) corresponds to a weathered near-surface horizon of gneissic conglomerates. This pattern likely reflects internal heterogeneity, with high resistivity values linked to large gneiss clasts forming a grain-supported framework, while lower values reflect the finer-grained sandstone matrix (cf. Fig. 5A–D). Kersantite, identified in profile ERT-7 on Ostrzew Hill, has a geometric mean resistivity of 937.3 m and a median value of 1002.0 m. These elevated resistivity values are consistent with the mafic composition and typically low porosity of unaltered kersantite (Fig. 9). Sandstones and mudstones of the Sokolec Formation intruded by this kersantite sill at the same locality also have relatively high resistivity values, likely due to thermal alteration related to intrusion emplacement (Fig. 9D).

Weathered gneiss has moderately high resistivity values, with geometric means ranging from ~187.1 m (ERT-7) to 764.0 m (ERT-5) and median values between 183.0 m (ERT-7) and 778.0 m (ERT-5), suggesting a partially altered structure of gneissic bedrock. In contrast, unweathered, massive gneisses consistently show higher resistivity, with geometric means ranging from 574.9 m (ERT-1) to 1750.8 m (ERT-3) and median values spanning from 594.3 m (ERT-1) to 1745.4 m (ERT-3), with several units exceeding 1000 m (e.g., 1433.3 m in ERT-1 profile and 1157.0 m in ERT-6 profile), reflecting a more compact, less porous lithology (Table 2; Figs. 8 and 9).

Unconsolidated Quaternary deposits (Q) display the lowest resistivity values among all lithological units, with geometric means ranging from 78.2 m (ERT-5) to 83.3 m (ERT-7) and median values from 73.5 m (ERT-7) to 77.9 m (ERT-5). These values are consistent with the geophysical response of fine-grained, unconsolidated, and water-saturated materials, primarily slope talus and deluvial tills. Such deposits are most notably developed in the Młynówka River valley near Glinno and, to a lesser extent, within the morphological depression separating Ostrzew Hill and Kokot Hill in the southern GG (as recorded in profile ERT-7; Fig. 9B, D).

Several narrow zones of anomalously low resistivity, marked by near-vertical indentations in the ERT profiles, were interpreted as fault zones (see Figs. 8 and 9). These include the Western Glinno Fault (FZ-1) and Eastern Glinno Fault (FZ-2), as well as two subsidiary fault zones – FZ-3 and FZ-4 – identified within the cemented sandstones and mudstones of the Sokolec Formation on Ostrzew Hill (profile ERT-7; Fig. 9D), which display steep lateral resistivity gradients. These anomalies are interpreted to represent water-saturated fault cores and zones of brecciation.

Statistical analysis shows that mean resistivity values in fault zones generally range from 114.1 to 452.8 m, with the majority of values falling between 257.7 m (ERT-5) and 293.3 m (ERT-1). Exceptions include markedly elevated resistivity recorded in cataclasites of FZ-1 in profile ERT-4 (geometric mean = 1106.2 m), likely reflecting massive and well-cemented fault-related rock, and low values in profile ERT-7 (FZ-3, 52.5 m) associated with a finer-grained, probably clayey, fault core. The resistivity contrast across fault zones also varies with lithology. In profiles ERT-4, ERT-5, and ERT-7, where fault zones intersect crystalline basement (i.e. gneisses), resistivity remains moderately elevated due to the inherently resistive nature of fractured metamorphic rocks. In contrast, in sedimentary successions intersected by FZ-1 in profiles ERT-1 and ERT-2, resistivity is markedly lower, consistent with the increased porosity, moisture retention, and finer grain size of fault zone (Fig. 8A, B).

STRUCTURAL ANALYSIS AND ARCHIVAL DATA

MESOSCALE FOLDS

During geological mapping of the GG, no meso-scale folds were observed in surface exposures. Only in the northern part of the graben (loc. 1; Fig. 4A), within a very limited exposure of Walim Formation sandstones dipping ~15° to the SW, small-scale folds were identified. These folds show probable south- or south-west vergence and are confined to a single bed ~40 cm thick, while the strata above and below remain undeformed (Fig. 5H). This localized deformation likely represents a case of soft-sediment deformation structure rather than tectonic folding.

Exposure-scale folds within the GG are otherwise known only from archival descriptions of research trenches excavated by Żakowa (1959, 1960). On the southwestern slope of Ostrzew Hill, within trench no. II, ~50 m long and 2–3 m deep, Żakowa (1960, p. 356) documented heterolithic packages of sandstones, mudstones, limestones and claystones of the Sokolec Formation, dipping predominantly ~20° to the NE (Fig. 10). In the northeastern part of the trench, Żakowa (1960) described mesoscopic folds forming a syncline–anticline pair, characterized by gentle, open geometry and nearly vertical axial planes. The fold limbs dip ~20° to the SW and NE, and the fold axes are subparallel to the general orientation of the GG, indicating nearly NE–SW-directed tectonic shortening.
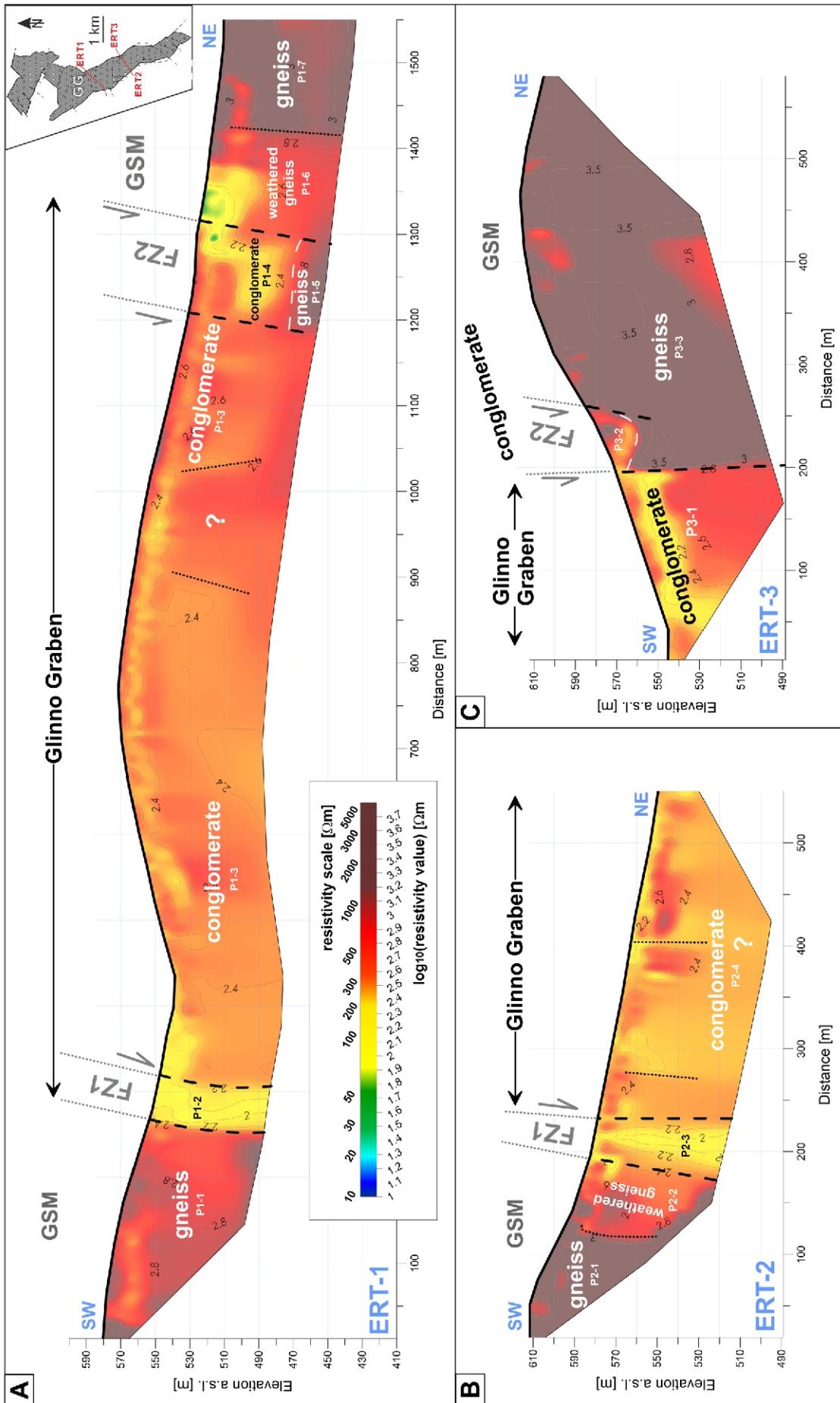
Fig. 8. Electrical resistivity tomography (ERT) cross-sections from the central part of the Glinno Graben, showing interpreted resistivity distributions alongside geological interpretations

See inset map in the upper right corner and Figures 2 and 4 for the locations of each cross-section
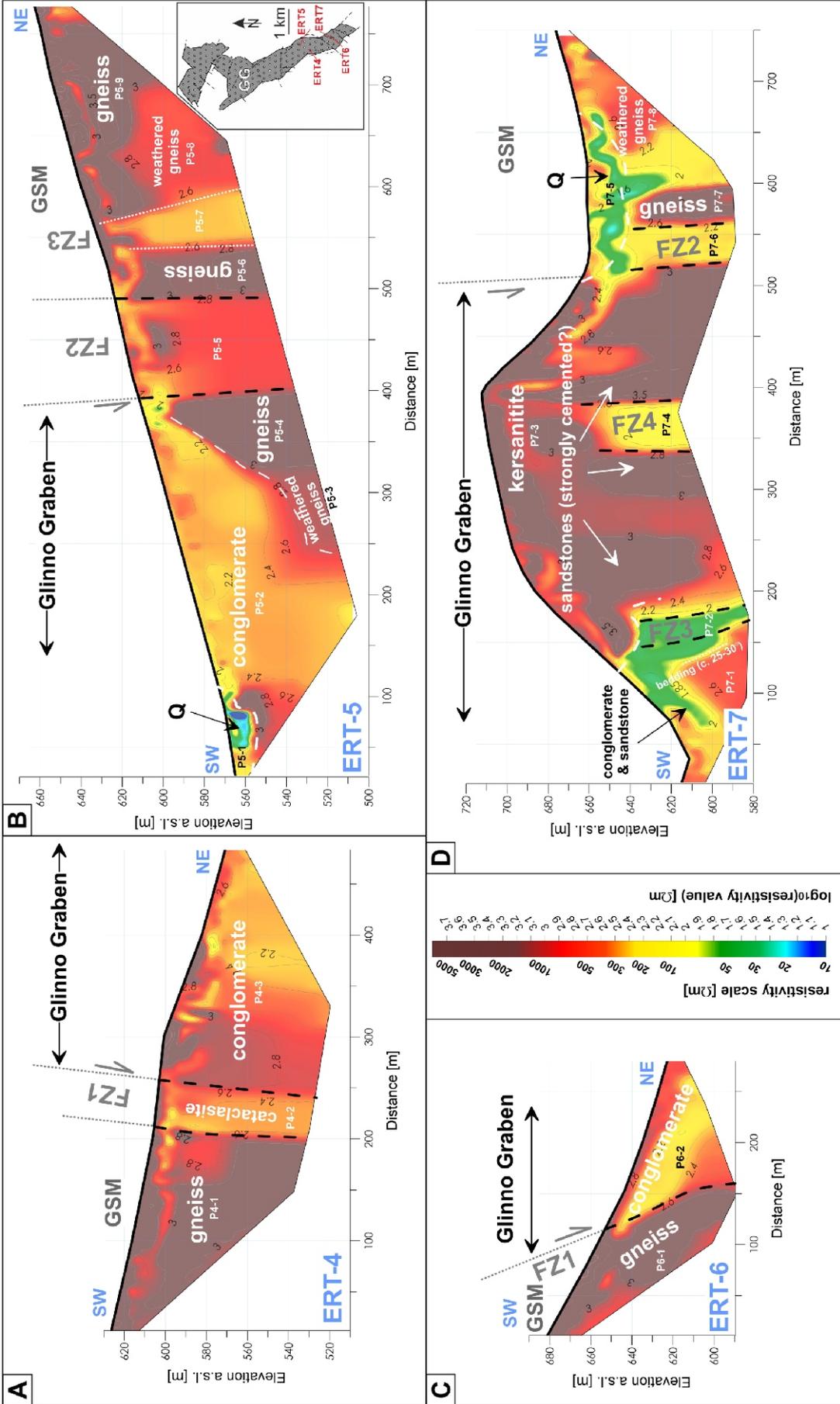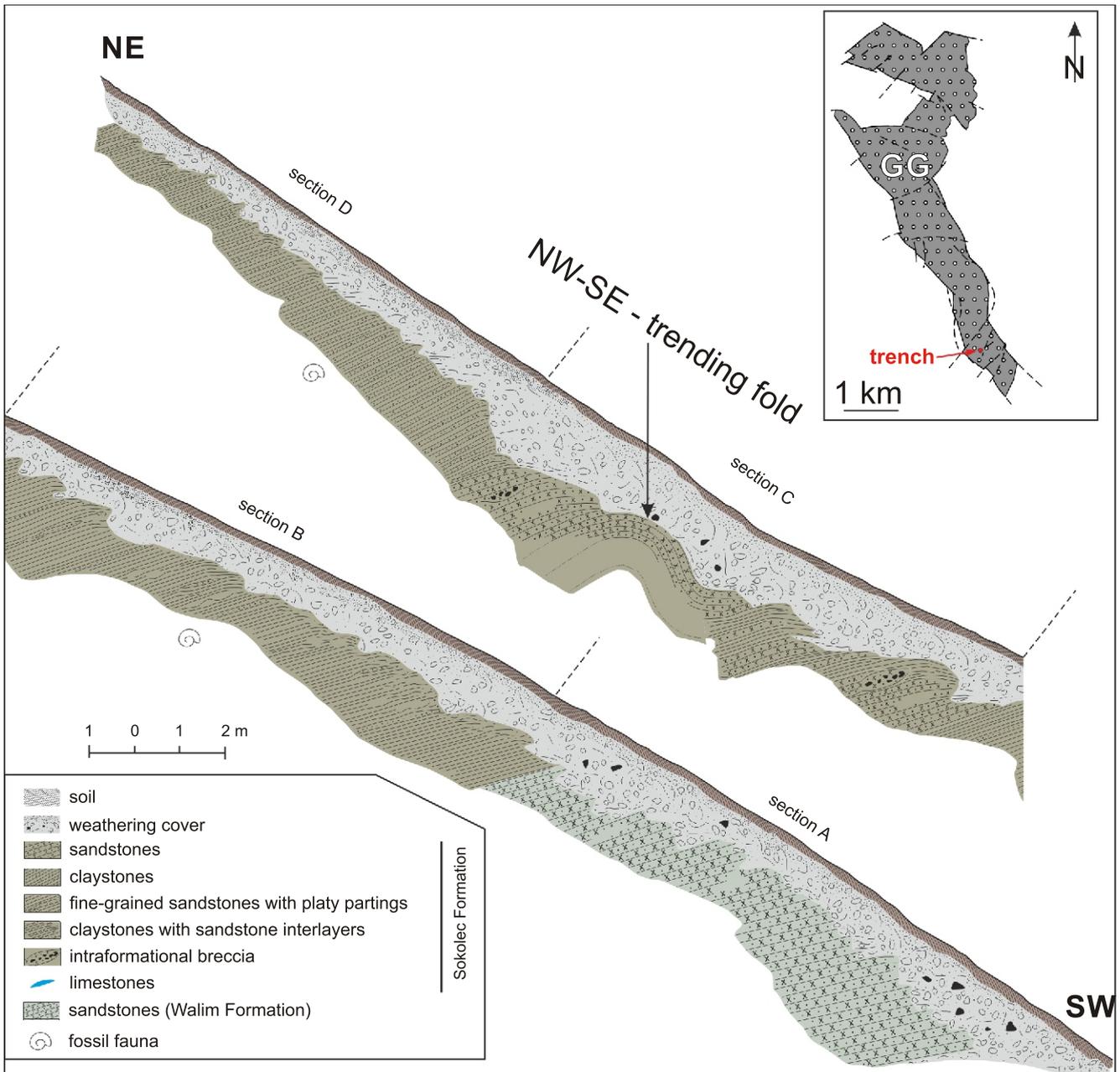
Fig. 9. Electrical resistivity tomography (ERT) cross-sections from the southern part of the Glinno Graben, showing interpreted resistivity distributions alongside geological interpretations

See inset map in the upper right corner and Figures 2 and 4 for the locations of each cross-section

Fig. 10. Profile of research trench on the southwestern slope of Ostrzew Hill, originally excavated by H. Żakowa in the late 1950s (redrawn from Żakowa, 1960, modified)

The trench was originally divided into four descriptive sections. Exposure-scale folds trending NW–SE are clearly visible in section C of the trench

No similar mesoscopic folds have been observed in sandstone exposures elsewhere on Ostrzew Hill. However, based on bedding attitude, a map-scale, fault-controlled syncline may be inferred in the southeasternmost part of the graben (Fig. 6). In contrast to the limited folding observed in the GG, exposure-scale folds are relatively common within the Mississippian marine Sokolec Formation in the adjacent Kamionki Graben (Żakowa and Żak, 1962; Kowalski and Pacanowski, 2025).

JOINTS AND FAULTS

The gneissic sandstones of the Walim Formation, occurring in several isolated exposures in the northern part of the GG (loc. 1; Figs. 4A and 5G), are affected by two conjugate joint sets, striking NW–SE and NE–SW, and referred to here as J_1 and J_2, respectively. A joint system with similar orientation is observed in the marine sandstones and mudstones of the Sokolec

T a b l e 2

Statistical parameters of resistivity for selected lithological units identified along ERT profiles in the Glinno Graben

Lithology	Number	Min.		Max.		Geometric mean		Median	
		log10 (resistivity) [Ωm]	Resistivity [Ωm]	log10 (resistivity) [Ωm]	Resistivity [Ωm]	log10 (resistivity) [Ωm]	Resistivity [Ωm]	log10 (resistivity) [Ωm]	Resistivity [Ωm]
Conglomerates	P1-3	1.91	81.5	3.13	1348.0	2.47	293.3	2.45	279.2
	P1-4	1.73	53.7	2.80	631.0	2.36	229.1	2.40	251.2
	P2-4	1.91	81.3	2.88	762.4	2.33	212.9	2.32	209.4
	P3-1	1.88	76.7	2.77	592.4	2.45	281.4	2.52	328.5
	P3-2	2.20	158.3	3.11	1280.8	2.63	431.4	2.65	441.9
	P4-3	1.83	66.9	4.16	14615.7	2.60	401.6	2.60	396.1
	P5-2	1.75	56.2	3.17	1491.0	2.37	233.8	2.33	215.0
	P6-2	1.99	98.3	3.34	2172.7	2.37	236.7	2.31	205.4
Conglomerates and sandstones	P7-1	1.51	32.5	2.71	515.6	2.15	140.5	2.17	148.8
Fault zones	P1-2 (FZ1)	1.87	73.7	2.52	327.7	2.06	114.1	2.03	108.2
	P2-3 (FZ1)	1.88	75.4	2.52	334.2	2.18	150.1	2.19	154.2
	P4-2 (FZ1)	2.04	110.1	3.58	3807.8	3.04	1106.2	3.04	1098.9
	P5-5 (FZ2)	1.98	94.8	3.10	1257.7	2.66	452.8	2.70	505.4
	P5-7 (FZ3)	2.19	153.8	3.66	4597.7	2.41	257.7	2.29	197.0
	P7-2 (FZ3)	1.57	37.5	2.09	121.8	1.72	52.5	1.71	50.8
	P7-4 (FZ4)	1.85	71.4	2.88	750.1	2.16	143.7	2.02	105.9
	P7-6 (FZ2)	1.80	62.7	2.79	610.7	2.15	140.9	2.12	131.1
Weathered gneisses	P1-6	1.71	51.1	3.04	1085.3	2.57	370.8	2.69	486.4
	P2-2	1.86	72.9	3.20	1596.5	2.62	418.9	2.61	405.4
	P5-3	2.75	566.4	2.97	924.1	2.88	764.0	2.89	778.0
	P5-8	2.39	247.4	3.82	6586.4	2.81	651.8	2.74	550.9
	P7-8	1.45	28.0	3.46	2894.8	2.27	187.1	2.26	183.0
Gneisses	P1-1	2.20	158.4	3.45	2822.2	2.76	574.9	2.77	594.3
	P1-5	2.62	418.6	3.04	1099.9	2.89	782.6	2.91	813.9
	P1-7	2.65	443.1	3.51	3225.7	3.01	1023.3	3.00	1002.6
	P2-1	2.54	344.2	3.57	3719.7	3.13	1355.6	3.16	1433.3
	P3-3	2.25	177.2	3.75	5621.7	3.24	1750.8	3.24	1745.4
	P4-1	2.04	110.1	3.58	3807.8	3.04	1106.2	3.04	1098.9
	P5-4	2.25	179.6	3.43	2686.6	3.19	1541.2	3.22	1651.7
	P5-6	2.17	147.1	3.69	4946.5	2.91	822.1	2.99	974.1
	P5-9	2.24	173.4	4.03	10597.4	3.21	1637.0	3.19	1565.6
	P6-1	2.05	111.8	3.92	8368.6	3.05	1123.2	3.06	1157.0
	P7-7	1.84	68.9	3.32	2080.9	2.84	685.1	2.97	934.2
Quaternary deposits	P5-1	0.33	2.1	3.01	1034.4	1.89	78.2	1.89	77.9
	P7-5	1.42	26.1	2.89	777.3	1.92	83.3	1.87	73.5
Kersanitites	P7-3	1.66	45.8	3.80	6351.5	2.97	937.3	3.00	1002.0

The table provides minimum and maximum resistivity values, as well as geometric mean and median resistivity (in Ωm) for each lithological unit interpreted on the basis of 2D inversion models. Profile numbers and lithological unit names correspond to labels used in Figures 8 and 9

Formation on Ostrzew Hill (loc. 4; Fig. 7E), as well as in the intersecting kersantite intrusions (loc. 5; Fig. 7E). These joints are generally oriented approximately perpendicular to bedding (or to the magmatic foliation in the kersantites) and display consistent strikes. The J_1 set strikes nearly NW–SE, parallel to the graben boundaries, while the J_2 set is oriented approximately NE–SW.

In exposures of the Sokolec Formation within the landslide body on the southern slopes of Ostrzew Hill (loc. 6), joint sets striking approximately N–S and W–E are observed. In addition,

strike-slip faults striking E–W have developed along fractures of the same orientation (Fig. 7C). Locally, these faults form well-defined, small-scale negative flower structures. Structural analysis of the joint surfaces suggests that these faults are localized along planes assigned to the J_2 set (originally striking NE–SW), which have been rotated clockwise. This rotation is interpreted as the result of downslope displacement of landslide blocks and their subsequent rotation around a vertical axis (Kowalski, 2018). These faults may represent high-angle Riedel shears (R-shears) associated with sinistral strike-slip move-

ment along NW–SE-oriented master faults. According to Kowalski (2018), fractures of the J_1 set within the sandstones and mudstones of the Sokolec Formation on the southwestern slope of Ostrzew Hill show clear evidence of sinistral strike-slip shearing. However, these exposures are currently inaccessible.

In the same landslide block exposure (loc. 6) on the southeastern slopes of Ostrzew Hill, normal faults striking nearly E–W and dipping southwards at angles of up to 80° have also been documented. These faults are most likely the result of gravitational processes; however, a tectonic origin cannot be entirely excluded. If of tectonic origin, these structures – similar to the sinistral strike-slip faults – may have originally been oriented nearly NE–SW, with their current geometry resulting from clockwise rotation during landslide displacement. Furthermore, in the southern part of the Ostrzew Hill massif, a depression trending NE–SW has been identified (Kowalski, 2018). This feature is interpreted as an extensional fracture, indicating segmentation of the massif along probable normal faults of similar orientation.

INTERPRETATION AND DISCUSSION

Given the scarcity of direct structural and stratigraphic evidence from the GG, its tectonic evolution is interpreted – based on the data presented in this study – within the broader context of regional deformation patterns established for adjacent, better-documented sectors of the NE Bohemian Massif. These surrounding regions are similarly partially overlain by syn- to post-Variscan sedimentary successions.

Drawing on the results of geological mapping, structural analysis, and shallow geophysical surveys, the model proposed here outlines a four-stage tectonic evolution of the GG (Fig. 11). This evolution closely mirrors the recently developed structural model for the adjacent Kamionki Graben (Kowalski and Pacanowski, 2025). The formation and development of the GG are interpreted to have initiated during the Carboniferous and progressed through multiple reactivation phases of inherited basement faults, episodic uplift, and erosional removal of the sedimentary cover of the GSM, continuing into the late Cenozoic.

NW–SE-trending meso-scale folds, identified within the Mississippian succession of the GG – particularly on the slopes of Ostrzew Hill – are interpreted as the result of end-Variscan compressional deformation. Similar fold styles are well documented in Carboniferous deposits preserved in both foreland and intramontane basins along the northeastern and eastern margins of the Bohemian Massif (Oberc, 1972; Hartley and Otava, 2001; Bábek et al., 2004, 2006; Mazur et al., 2006, 2010; Narkiewicz, 2007, 2020; Tomek et al., 2019). Mesoscale folds have also been described from the Paleozoic sedimentary successions forming the Variscan external fold-and-thrust belt in western and central Poland. Seismic reflection profiles and borehole data reveal that these successions are dominated by imbricate thrust stacks and moderately to steeply inclined folds trending WNW–ESE to NW–SE, which reflect northeast-directed shortening and the progressive propagation of the Variscan deformation front during the late Carboniferous (Mazur et al., 2010, 2020; Krzywiec et al., 2017; Tomaszczyk and Jarosiński, 2017; Mazur and Schulmann, 2025). This structural geometry is consistent with the regional end-Variscan stress field reconstructed across the northeastern termination of the belt, suggesting that the GG area records a comparable style of folding related to this compressional phase.

At the regional scale, the fold tectonics affecting the Mississippian strata overlying the GSM correspond to the deformation style observed in the adjacent Bardo Unit (Oberc, 1972). According to Oberc, the Bardo succession experienced an initial phase of folding at the transition from the early to late Carboniferous, forming E–W- to NW–SE-trending structures. These were later overprinted by late Carboniferous refolding, which produced NE–SW to N–S-oriented folds superimposed on the earlier fabric (Oberc, 1972). The E–W- to NW–SE-trending initial folds are attributed to deformation associated with the late-Variscan ("*Sudetic*") phase of E-W to NE–SW compression. The geometry of meso-scale folds documented in the GG – particularly within the Sokolec Formation at Ostrzew Hill – closely mirrors that observed in the southern sector of the Kamionki Graben, where WNW–ESE to W–E, and less commonly NW–SE-trending, exposure-scale folds and associated reverse faults have been reported (Kowalski and Pacanowski, 2025). The consistent structural patterns between the two grabens suggest that both underwent comparable phases of deformation, likely transpressional in character, controlled by the reactivation of inherited basement faults within the GSM (Kowalski and Pacanowski, 2025). Late Paleozoic dextral movements along major crustal shear zones in the northeastern Bohemian Massif, active during the final stages of the Variscan orogeny, have been widely documented (Aleksandrowski, 1995; Aleksandrowski et al., 1997; Žák et al., 2018; Tomek et al., 2019). These displacements most likely occurred on a broader scale as a consequence of oblique convergence between Gondwana-derived microcontinents and Laurussia (Mazur et al., 2006; Hofmann et al., 2009; Franke et al., 2017; Edel et al., 2018; Žák et al., 2018; Tomek et al., 2019; Martínez-Catalán et al., 2021).

The sinistral strike-slip faults observed in the Sokolec Formation at Ostrzew Hill are interpreted as the product of a second deformation phase associated with the initial tectonic development of the GG. The formation of the graben likely followed shortly after the folding of the Carboniferous strata and is attributed to a period of regional uplift and erosion during the late Carboniferous to early Permian. The strike-slip faults observed within the landslide-displaced blocks affected clockwise-rotated surfaces of the J_2 joint set, originally oriented NE–SW and parallel to the graben boundaries, and may represent high-angle Riedel (R) shears. Sinistral shearing along NW-SE-oriented J_1 joints on the southwestern slopes of Ostrzew Hill was previously documented by Kowalski (2018), suggesting that this deformation pattern is part of a broader, regionally significant trend. Further support comes from the adjacent Kamionki Graben, where NNW–SSE to NNE–SSW-striking strike-slip faults (fault population II of Kowalski and Pacanowski, 2025) show comparable geometry and are attributed to a late Carboniferous–early Permian transtensional regime, characterized by NE–SW to WNW–ESE-oriented extension. Notably, this proposed kinematic phase aligns with interpreted late Carboniferous–early Permian sinistral displacement along the Głuszyca Fault – a segment of the Intra-Sudetic Fault System – which runs parallel to both grabens and forms the southwestern boundary of the GSM (Aleksandrowski, 1995; Aleksandrowski et al., 1997). Additionally, the emplacement of NW–SE to NNW–SSE-oriented kersantite and rhyolite dykes within the GSM (Grocholski, 1967; Awdankiewicz, 2007), along with coeval volcanic and subvolcanic bodies in the adjacent Intra-Sudetic Basin (Awdankiewicz, 1999, 2022), appears genetically linked to this regional extensional tectonic regime. According to Nádaskay et al. (2024), during the middle Pennsylva-
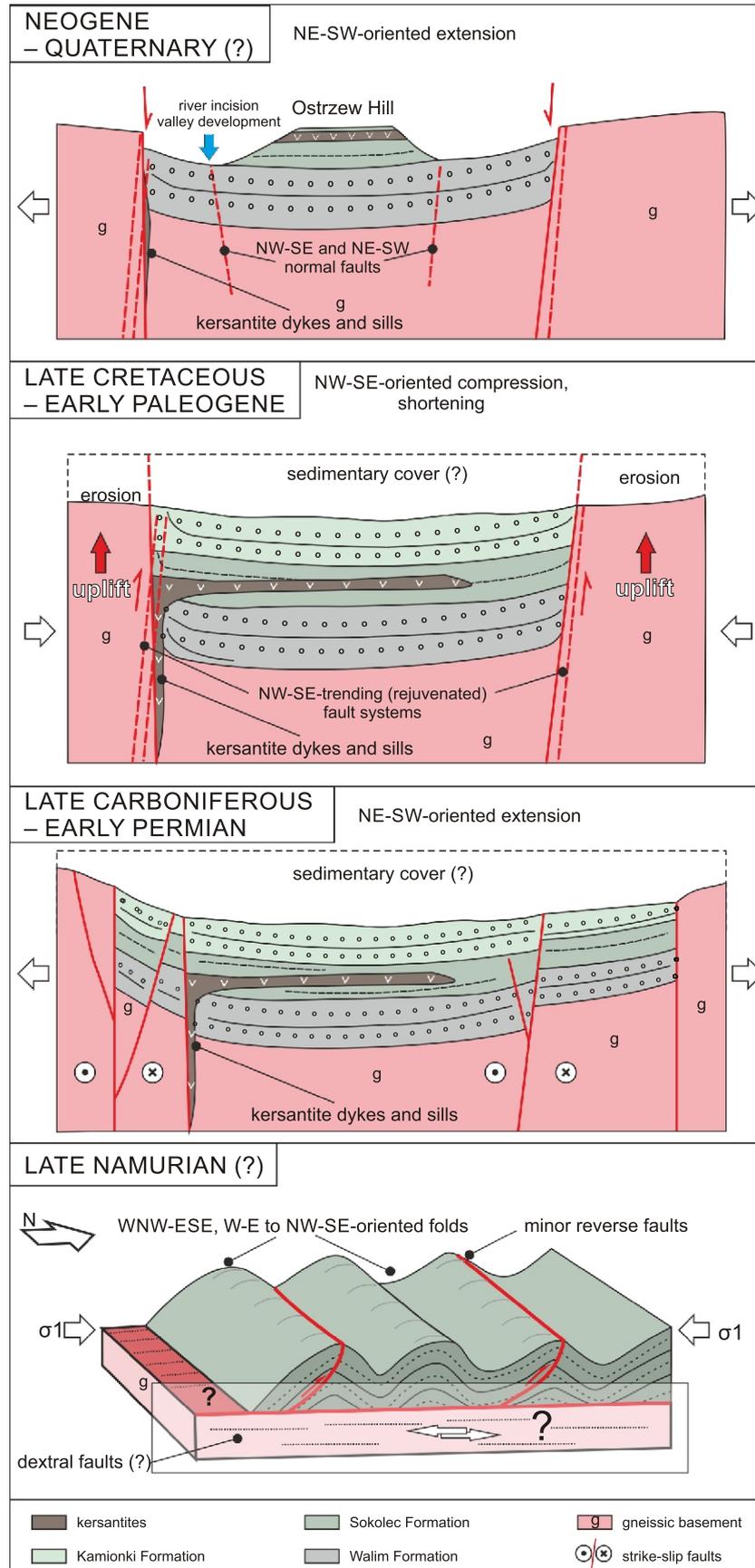
Fig. 11. Schematic model illustrating the deformation of the Mississippian succession in the Glinno Graben

The diagram depicts the inferred late Namurian folding phase after Kowalski and Pacanowski (2025).
For detailed discussion and additional context, refer to the main text

nian to early Permian (Moscovian–early Asselian; ~310–300/ 298 Myr), sinistral strike-slip deformation along NW–SE-oriented fault zones in the northeastern Bohemian Massif was likely triggered as a far-field effect of the Uralian orogeny.

Reconstructing the tectono-sedimentary evolution of the GSM from the Permian to Early Cretaceous remains highly challenging due to the absence of preserved sedimentary cover and limited structural evidence. While Lower Triassic deposits are well documented in the adjacent Intra-Sudetic Basin, the GSM likely acted as a sediment source during that time (Mroczkowski and Mader, 1985; Kowalski, 2020). However, it remains unclear whether any sedimentary succession covered the mountainous portion of the massif or its continuation within the Fore-Sudetic Block. Geophysical data indicate that structural levels exposed in the foreland are ~5 km deeper than those in the Sudetic part, raising the possibility that sedimentary rocks never accumulated there, or were entirely removed by post-Carboniferous erosion (Oberc, 1972). Based on apatite fission-track data, Aramowicz et al. (2006) proposed that the GSM may once have been buried beneath a significant thickness of upper Carboniferous–Permian, or younger (?) deposits, suggesting a notable post-Variscan burial event prior to its final exhumation.

The presence of Jurassic and Early Cretaceous strata over the GSM remains uncertain, and if such cover existed, it has since been eroded. Outcrops of these rocks are limited to areas west of the Elbe Fault Zone (Valečka, 2019, Nádaskay et al., 2024), raising doubts as to whether the GSM was ever covered during this time. Although extensional reactivation of Variscan strike-slip faults and localized subsidence during the Middle Jurassic–Early Cretaceous has been proposed in the NE Bohemian Massif (Nádaskay et al., 2019), palaeogeographic reconstructions generally exclude the GSM from these depositional areas. During the Late Cretaceous, the GSM clearly emerged as part of the Eastern Sudetic Island, supplying clastic material to adjacent basins (Wojewoda, 1997; Biernacka, 2012; Kowalski, 2021b).

During the Late Cretaceous to early Paleogene, the elevated part of the GSM underwent significant tectonic uplift along two major basement faults: the Sudetic Boundary Fault (NE) and the Głuszyca Fault (SW). This uplift is attributed to NE–SW-oriented compressional stress resulting from the convergence of the African, Iberian, and European plates, transmitted as far-field effects across considerable distances from the active orogenic fronts (Rosenbaum et al., 2002; Mazur et al., 2005; Kley and Voigt, 2008). The result was regional-scale inversion of Permo-Mesozoic and older basins, forming a wide NW–SE trending belt of basement uplifts and associated depressions bounded by reactivated high-angle faults in Central Europe. Prominent structural highs within this belt include the inverted Lower Saxony Basin, Harz Mountains, Flechtingen High, Thuringian Forest and its Bavarian prolongations, and the Lusatian–Sudetic High (Voigt, 2009; Kley and Voigt, 2008). While Voigt et al. (2021) suggested that tectonic inversion in Central Europe began as early as ~95 Ma (Cenomanian), in the Intra-Sudetic Basin the youngest preserved Cretaceous strata are of Lower Coniacian age (~89–87 Ma; Wojewoda, 1997; Kowalski, 2021b). This implies that tectonic uplift of the GSM and its surroundings may have initiated somewhat later, likely during the late Coniacian to Santonian (~87–84 Ma), following the termination of sedimentation in the basin – provided that younger deposits were not subsequently eroded, which remains a possibility. This interpretation aligns with the thermochronological findings of Danišík et al. (2012), who argued that reverse faults and low-angle thrusts were active across the Sudetic region during the ~85–70 Myr interval, indi-

cating a regional compressional phase consistent with the Late Cretaceous to early Paleogene deformation event. Palaeostress indicators from reverse faults in the nearby Kamionki Graben suggest NW–SE-directed compression, consistent with data documenting this deformation phase in the northeastern Bohemian Massif and the Sudetes region (Pešková et al., 2010; Coubal et al., 2015; Nováková, 2015; Sobczyk et al., 2015, 2019; Kowalski, 2021; Głuszyński and Aleksandrowski, 2022; Kowalski and Pacanowski, 2025). Thermochronological constraints indicate removal of ~4–8 km of overburden from the GSM during this episode, with ~4 km of denudation also recorded in the Intra-Sudetic Basin (Aramowicz et al., 2006; Botor et al., 2019). Sobczyk et al. (2015) further postulated that burial depths within the axial part of the Intra-Sudetic Basin reached up to 5.5–6 km, implying a comparable magnitude of subsequent exhumation during post-Cretaceous uplift and basin inversion. Although exposure evidence in the GG is limited, map-scale folds within the Mississippian succession, particularly the NW–SE trending syncline in the southernmost part of the graben, likely reflect the same compressional phase. The large-scale folds observed in other parts of the GG most likely also formed during this compressional event. However, the bedding is poorly expressed in the gneissic conglomerates, where its identification is particularly challenging due to the massive structure and weathering, a difficulty compounded by the near-total absence of fresh exposures.

Based on field observations conducted in the GG, a subsequent episode of extensional deformation is proposed, marked by the development of normal faults that likely represent the youngest tectonic dislocations affecting the graben structure. These faults are oriented either parallel or perpendicular to the nearby NW–SE-trending Sudetic Boundary Fault (Oberc and Dyjor, 1969; Krzyszkowski and Pijet, 1993; Krzyszkowski et al., 1995; Badura et al., 2007; Różycka et al., 2021; Migoń et al., 2023), suggesting that a late-stage extensional regime has been superimposed on pre-existing structural discontinuities. On the southern slopes of Ostrzew Hill (loc. 6), both normal faults and extensional fractures – clearly expressed in present-day terrain morphology – have been documented. Additionally, two landslides have been identified in this area, whose development appears closely linked to the fault-controlled bedrock architecture. These faults, along with other dislocations that have contributed to the internal compartmentalization of the GG – such as NE–SW-oriented faults dissecting both the Kurasz Fault and the Northern Glinno Fault – are most likely associated with Neogene to Quaternary fault activity previously reported along the Sudetic Boundary Fault (Krzyszkowski et al., 1995; Krzyszkowski and Bowman, 1997; Migoń and Łach, 1998; Badura et al., 2007; Štěpančíková et al., 2010, 2011; Różycka et al., 2021; Migoń et al., 2023) and subordinate fault systems within the GSM. This late-stage faulting appears to have exerted a substantial influence on the local drainage network. The course of the Młynówka River valley in the central and southern sectors of the graben, as well as the headwater zone of the Bojanicka Woda stream in its northern part, closely follows morphological depressions that coincide with mapped fault zones. This spatial correspondence suggests that neotectonic movements along normal faults may have played a key role in controlling fluvial incision and valley alignment in the GG area. Moreover, the isolated position of Ostrzew Hill situated in the axial zone of the graben likely reflects a combination of structural preservation and differential erosion, controlled probably by late-stage normal faulting. Hence, Ostrzew Hill may represent an erosional remnant bounded by NE–SW-oriented faults that segmented the graben floor during Neogene to Quaternary extensional deformation.

Another important issue that must be addressed in the context of the Neogene to Quaternary evolution of the GG concerns the nature and kinematics of the Sudetic Boundary Fault, particularly with respect to the earlier, possible strike-slip displacements along this structure. According to Cwojdziński and Żelaźniewicz (1995), the absence of a pronounced offset in the mapped boundaries of the GSM along the fault suggests that previously proposed strike-slip displacements along this structure were likely minor or of limited geological significance. Furthermore, Cwojdziński et al. (1995) and Żelaźniewicz et al. (1997), based on interpretations of the GB-2A seismic reflection profile, proposed that both the Sudetic Boundary Fault and the Intra-Sudetic Fault functioned as multiply reactivated listric faults. Importantly, the crystalline basement of the GSM extends southwards beneath the Devonian strata of the northern Bardo Unit (Chorowska et al., 1992) and likely also underlies parts of the Świebodzice Unit (Porębski, 1981, 1990), beyond the currently mapped extent of the mountainous massif. This structural configuration implies that the apparent continuity of GSM boundaries may be misleading and potentially obscured by vertical (dip-slip) fault reactivation during the Neogene to Quaternary tectonic phase. Consequently, the absence of a visible lateral offset in plan view does not preclude the occurrence of strike-slip displacements during earlier stages of the tectonic evolution of the Sudetic Boundary Fault. Such displacements likely occurred primarily along the Intra-Sudetic Fault, which has been widely recognized as a major zone of late Paleozoic strike-slip deformation.

SUMMARY AND CONCLUSION

The Glinno Graben is a well-defined, fault-controlled tectonic feature developed atop the crystalline basement of the metamorphic Góry Sowie Massif, comprising folded syn- to late-orogenic Mississippian strata. Its structural evolution reflects the complex, late- to post-Variscan tectonosedimentary history of the northeastern Bohemian Massif.

This study provides an integrated structural, geomorphological, and geophysical analysis of the graben, based on detailed geological mapping, LiDAR-based terrain analysis, and two-dimensional Electrical Resistivity Tomography (ERT). The preserved Carboniferous succession – comprising gneissic conglomerates and sandstones of the Walim Formation and marine deposits of the Sokolec Formation – is locally intruded by NW–SE- to NNW–SSE-trending kersantite dykes and sills, indicating late-Variscan magmatic activity. The Glinno Graben consists of at least three fault-bounded tectonic subunits, delineated by major dislocations including the Western, Eastern, Kurasz, and Northern Glinno faults. ERT imaging reveals a pronounced contrast between the resistive crystalline basement and the more conductive sedimentary infill, allowing for high-resolution mapping of fault zones and precise characterization of the overall graben geometry.

Structural data and regional correlations support a four-stage deformation model of the graben. The first phase – represented by NW–SE-trending meso-scale folds in the Mississippian succession – is attributed to end-Variscan NNE–SSW to NE–SW shortening. The meso-scale folds likely formed under compressional or transpressional (dextral?) regimes. The second phase involved sinistral strike-slip faulting during late Carboniferous to early Permian transtension. This event is reflected in fault planes dissecting the Sokolec Forma-

tion and aligns kinematically with sinistral deformation in the Kamionki Graben and along the nearby Intra-Sudetic Fault. It also corresponds with the emplacement of kersantite dykes and associated igneous activity in the GSM and Intra-Sudetic Basin.

A third, regionally significant tectonic phase occurred during the Late Cretaceous to early Paleogene, when NW–SE-directed far-field compressional stress – generated by the convergence of the African, Iberian, and European plates – reactivated inherited high-angle basement faults and triggered the inversion of Permo-Mesozoic basins and older tectonic structures in Central Europe. This stress regime induced crustal shortening within the northeastern Bohemian Massif and led to the uplift of the mountainous part of the GSM, particularly along the Sudetic Boundary Fault and the Głuszyca Fault. It also caused extensive erosion of the massif and its sedimentary cover. Reverse faults and large-scale folds observed within the Mississippian succession of the GG – although only locally exposed – are likely attributable to this compressional phase and are consistent with palaeostress reconstructions from the adjacent Kamionki Graben.

The final phase of deformation is characterized by Neogene to Quaternary NW-SE-oriented extension, manifested as high-angle normal faults and extensional fractures – particularly in the southern sector of the graben in Ostrzew Hill. These structures, locally rotated within landslide bodies, show orientations either parallel or perpendicular to the Sudetic Boundary Fault, suggesting a late-stage extensional regime superimposed on older faults. In addition to controlling the development of slope instabilities, these graben-parallel faults appear to have influenced the alignment and incision of the local drainage network. The Młynówka River valley and Bojanicka Woda headwaters both coincide with fault-controlled depressions, indicating a possible neotectonic imprint on modern topography.

Importantly, the proposed structural evolution of the Glinno Graben, involving repeated episodes of fault reactivation from the Carboniferous to Quaternary, is consistent with the deformation history reconstructed for the adjacent Kamionki Graben. These findings emphasize the persistent regional role of inherited basement faults and their long-term tectonic reactivation in influencing the structural framework of the northeastern Bohemian Massif.

REFERENCES

ABEM, 2011. Terraloc Pro. Instruction Manual. Available online: https://wwwguidelinegeoc.cdn.triggerfish.cloud/uploads/2016/03/Terraloc-Pro-Instruction-Manual.pdf (accessed on 10 July 2022)

Aleksandrowski, P., 1995. The significance of major strike-slip displacements in the development of Variscan structure of the Sudetes (SW Poland) (in Polish with English summary). Przegląd Geologiczny, **43**: 745–754.

Aleksandrowski, P., Kryza, R., Mazur, S., Pin, C., Zalasiewicz, J.A., 1999. The Polish Sudetes: Caledonian or Variscan? Transactions of the Royal Society of Edinburgh: Earth Sciences, **90**: 127–146; https://doi.org/10.1017/S0263593300007197

Aleksandrowski, P., Kryza, R., Mazur, S., Żaba, J., 1997. Kinematic data on major Variscan strike-slip faults and shear zones in the Polish Sudetes, northeast Bohemian Massif. Geological Magazine, **133**: 727–739; https://doi.org/10.1017/S0016756897007590

Aramowicz, A., Anczkiewicz, A., Mazur, S., 2006. Fission-track dating of apatite from the Góry Sowie Massif, Polish Sudetes, NE Bohemian Massif: Implications of post-Variscan denudation and uplift. Neues Jahrbuch für Mineralogie Abhandlungen, **182**: 221–229; https://doi.org/10.1127/0077-7757/2006/0046

Augustyniak, K., Grocholski, A., 1968. Geological structure and outline of the development of the Intra-Sudetic depression. Biuletyn Instytutu Geologicznego, **17**: 87–111.

Awdankiewicz, M., 1999. Volcanism in a late Variscan intramontane trough: Carboniferous and Permian volcanic centres of the Intra-Sudetic Basin, SW Poland. Geologia Sudetica, **32**: 13–47.

Awdankiewicz, M., 2007. Late Palaeozoic lamprophyres and associated mafic subvolcanic rocks of the Sudetes (SW Poland): petrology, geochemistry and petrogenesis. Geologia Sudetica, **39**: 11–97.

Awdankiewicz, M., 2022. Polyphase Permo-Carboniferous magmatism adjacent to the Intra-Sudetic Fault: constraints from U–Pb SHRIMP zircon study of felsic subvolcanic intrusions in the Intra-Sudetic Basin, SW Poland. International Journal of Earth Sciences, **111**: 2199–2224; https://doi.org/10.1007/s00531-022-02232-y

Awdankiewicz, M., Kryza, R., Turniak, K., Ovtcharova, M., Schaltegger, U., 2021. The Central Sudetic Ophiolite (European Variscan Belt): precise U–Pb zircon dating and geotectonic implications. Geological Magazine, **158**: 555–566; https://doi.org/10.1017/S0016756820000722

Bábek, O., Mikuláš, R., Zapletal, J., Lehotský, T., 2004. Combined tectonic-sediment supply-driven cycles in a Lower Carboniferous deep-marine foreland basin, Moravice Formation, Czech Republic. International Journal of Earth Sciences, **93**: 241–261; https://doi.org/10.1007/s00531-004-0388-5

Bábek, O., Tomek, Č., Melichar, R., Kalvoda, J., Otava, J., 2006. Structure of unmetamorphosed Variscan tectonic units of the southern Moravo-Silesian zone, Bohemian Massif: a review. Neues Jahrbuch für Geologie und Paläontologie Abhandlungen, **239**: 37–75; https://doi.org/10.1127/njgpa/239/2006/37

Badura, J., Zuchiewicz, W., Štěpančíková, P., Przybylski, B., Kontny, B., Cacoń, S., 2007. The Sudetic Marginal Fault: a young morphophotectonic feature at the NE margin of the Bohemian Massif, Central Europe. Acta Geodynamica et Geomaterialia, **4**: 7–29.

Bania, G., Mościcki, W.J., Golonka, J., 2024. ERT field survey supported with numerical and analogue modeling applied to study a fragment of the Pieniny Klippen Belt (Spisz Pieniny Mountains, southern Poland). Geological Quarterly, **68**, 22; https://doi.org/10.7306/gq.1750

Biernacka, J., 2012. Provenance of Upper Cretaceous quartz-rich sandstones from the North Sudetic Synclinorium, SW Poland: constraints from detrital tourmaline. Geological Quarterly, **56**: 333–344; https://doi.org/10.7306/gq.1024

Binley, A., Slater, L., 2020. Resistivity and Induced Polarization: Theory and Applications to the Near-Surface Earth. Cambridge University Press; https://doi.org/10.1017/9781108685955

Bossowski, A., Ihnatowicz, A., 2006. Geological Atlas of the Lower Silesian Coal Basin 1:100 000 (in Polish with English summary). Polish Geological Institute, Warszawa.

Botor, D., Anczkiewicz, A.A., Mazur, S., Siwecki, T., 2019. Post-Variscan thermal history of the Intra-Sudetic Basin (Sudetes, Bohemian Massif) based on apatite fission track analysis. International Journal of Earth Sciences, **108**: 2561–2576; https://doi.org/10.1007/s00531-019-01777-9

Bröcker, M., Żelaźniewicz, A., Enders, M., 1998. Rb–Sr and U–Pb geochronology of migmatitic gneisses from the Góry Sowie (West Sudetes, Poland): the importance of Mid–Late Devonian metamorphism. Journal of the Geological Society, **155**: 1025–1036; https://doi.org/10.1144/gsjgs.155.6.1025

Caputo, R., Piscitelli, S., Oliveto, A., Rizzo, E., Lapenna, V., 2003. The use of electrical resistivity tomographies in active tectonics: examples from the Tyrnavos Basin, Greece. Journal of Geodynamics, **36**: 19–35; https://doi.org/10.1016/S0264-3707(03)00036-X

Chambers, J.E., Kuras, O., Meldrum, P.I., Ogilvy, R.D., Hollands, J., 2006. Electrical resistivity tomography applied to geologic, hydrogeologic, and engineering investigations at a former waste-disposal site. Geophysics, **71**: B231–B239; https://doi.org/10.1190/1.2360184

Chorowska, M., Fedorowski, J., Radlicz, K., 1992. Famennian and Tournaisian deposits from the Zdanów IG 1 borehole (Sudetes). Geological Quarterly, **36** (1): 1–32.

Coubal, M., Málek, J., Adamovič, J., Štěpančíková, P., 2015. Late Cretaceous and Cenozoic dynamics of the Bohemian Massif inferred from the paleostress history of the Lusatian Fault Belt. Journal of Geodynamics, **87**: 26–49; https://doi.org/10.1016/j.jog.2015.02.006

Cwojdziński, S., Żelaźniewicz, A., 1995. Crystalline basement of the Fore-Sudetic Block (in Polish with English summary). In: Przewodnik LXVI Zjazdu Polskiego Towarzystwa Geologicznego (eds. S. Cwojdziński, S. Dyjor, S. Staśko and A. Żelaźniewicz): 11–28.

Cwojdziński, S., Młynarski, S., Dziewińska, L., Jóźwiak, W., Zientara, P., Baziuk, T., 1995. GB-2A – First seismic profile of the deep reflection study in Lower Silesia (SW Poland) (in Polish). Przegląd Geologiczny, **43**: 727–737.

Cymerman, Z., 1988. Structural development of the Góry Sowie metamorphic terrain in the vicinity of Piława Górna, the Sudetes (in Polish with English summary). Geologia Sudetica, **23**: 107–132.

Cymerman, Z., 1989. Structural evolution of the Góry Sowie unit in the area of northern part of the Bielawa Hills, Sudetes Mts. Geologia Sudetica, **24**: 191–283.

Cymerman, Z., 1998. The Góry Sowie Terrane: a key to understanding the Palaeozoic evolution of the Sudetes area and beyond. Geological Quarterly, **42** (3): 379–400.

Cymerman, Z., Brytan, J., Kowalski, A., 2023. Szczegółowa mapa geologiczna Sudetów w skali 1:25 000, arkusz Walim (834D), PIG-PIB Warszawa (in Polish). CAG PIG, Warszawa, CBDG: 5970/2025.

Dahlin, T., Zhou, B., 2004. A numerical comparison of 2D resistivity imaging with 10 electrode arrays. Geophysical Prospecting, **52**: 379–398; https://doi.org/10.1111/j.1365-2478.2004.00423.x

Danišík, M., Štěpančíková, P., Evans, N., 2012. Constraining long-term denudation and faulting history in intraplate regions by multisystem thermochronology: An example of the Sudetic Marginal Fault (Bohemian Massif, central Europe). Tectonics, **31**, 2003; https://doi.org/10.1029/2011TC003012

Dathe, E., Finckh, L., 1924. Geologische Karte von Preußen und benachbarten Bundesstaaten 1:25 000. Blatt Charlottenbrunn, Lieferung 254. Preußischen Geologischen Landesalstalt, Berlin.

Davis, J.C., Sampson, R.J., 1986. Statistics and data analysis in geology. Wiley, New York.

Don, J., 2003. The problem of „diastrophic" blocks in the marginal parts of the Late Cretaceous Nysa Kłodzka graben, the Sudetes, SW Poland. Geologia Sudetica, **35**: 61–67.

Don, J., Gotowała, R., 2008. Tectonic evolution of the late Cretaceous Nysa Kłodzka Graben, Sudetes, SW Poland. Geologia Sudetica, **40**: 51–63.

Drahor, M.G., Berge, M.A., 2017. Integrated geophysical investigations in a fault zone located on southwestern part of İzmir city, Western Anatolia, Turkey. Journal of Applied Geophysics, **136**: 114–133; https://doi.org/10.1016/j.jappgeo.2016.10.021

Dubińska, E., Gunia, P., 1997. The Sudetic ophiolite: current view on its geodynamic model. Geological Quarterly, **41** (1): 1–20.

Ducut, J.D., Alipio, M., Go, P.J., II, R.C., Vicerra, R.R., Bandala, A., Dadios, E., 2022. A review of Electrical Resistivity Tomography Applications in underground imaging and object detection. Displays, **73**, 102208; https://doi.org/10.1016/j.displa.2022.102208

Dziedzic, K., Teisseyre, A.K., 1990. The Hercynian molasse and younger deposits in the Intra-Sudetic Depression, SW Poland. Neues Jahrbuch für Geologie und Paläontologie Abhandlungen, **179**: 285–305.

Edel, J.B., Schulmann, K., Lexa, O., Lardeaux, J., 2018. Late Palaeozoic palaeomagnetic and tectonic constraints for amalgamation of Pangea supercontinent in the European Variscan belt. Earth-Science Reviews, **177**: 589–612; https://doi.org/10.1016/j.earscirev.2017.12.007

Farr, T.G., Rosen, P.A., Caro, E., Crippen, R., Duren, R., Hensley, S., Kobrick, M., Paller, M., Rodriguez, E., Roth, L., Seal, D., Shaffer, S., Shimada, J., Umland, J., Werner, M., Oskin, M., Burbank, D., Alsdorf, D., 2007. The Shuttle Radar Topography Mission. Reviews of Geophysics, **45**, RG2004; https://doi.org/10.1029/2005RG000183

Fischer, T., Štěpančíková, P., Karousová, M., Tábořík, P., Flechsig, C., Gaballah, M., 2012. Imaging the Mariánské Lázně Fault (Czech Republic) by 3-D ground-penetrating radar and electric resistivity tomography. Studia Geophysica et Geodaetica, **56**: 1019–1036.

Franke, W., Żelaźniewicz, A., 2023. Variscan evolution of the Bohemian Massif (Central Europe): Fiction, facts and problems. Gondwana Research, **124**: 351–377; https://doi.org/10.1016/j.gr.2023.06.012

Franke, W., Cocks, L.R.M., Torsvik, T.H., 2017. The Palaeozoic Variscan oceans revisited. Gondwana Research, **48**: 257–284; https://doi.org/10.1016/j.gr.2017.03.005

Głuszyński, A., Aleksandrowski, P., 2022. Late Cretaceous-Early Palaeogene inversion-related tectonic structures at the NE margin of the Bohemian Massif (SW Poland and northern Czechia). Solid Earth, **13**: 1219–1242; https://doi.org/10.5194/se-13-1219-2022

Górecka-Nowak, A., Muszer, J., Maćko, A., 2025. The Carboniferous of the Sudetes in the light of new biostratigraphic studies (in Polish with English summary). Przegląd Geologiczny, **73**: 776–783; https://doi.org/10.7306/2025.83

Grocholski, W., 1962. Szczegółowa Mapa Geologiczna Sudetów w skali 1:25 000, arkusz Walim (in Polish). Wydaw. Geol., Warszawa.

Grocholski, W., 1965. Objaśnienia do Szczegółowej Mapy Geologicznej Sudetów w skali 1:25 000, arkusz Walim (in Polish). Wydaw. Geol., Warszawa.

Grocholski, W., 1967. Structure of the Sowie Mts. (in Polish with English summary). Geologia Sudetica, **3**: 181–249.

Gunia, T., 1999. Microfossils from the high-grade metamorphic rocks in the Góry Sowie Mts. (Sudetes area) and their stratigraphical importance. Geological Quarterly, **43** (4): 519–536.

Hartley, A.J., Otava, J., 2001. Sediment provenance and dispersal in a deep marine foreland basin: the Lower Carboniferous Culm Basin, Czech Republic. Journal of the Geological Society, **158**: 137–150; https://doi.org/10.1144/jgs.158.1.137

Haydukiewicz, J., 1990. Stratigraphy of Paleozoic rocks of the Góry Bardzkie and some remarks on their sedimentation (Poland). Neues Jahrbuch für Geologie und Paläontologie Abhandlungen, **179**: 275–284.

Hofmann, M., Linnemann, U., Gerdes, A., Ullrich, B., Schauer, M., 2009. Timing of dextral strike-slip processes and basement exhumation in the Elbe Zone (Saxo-Thuringian Zone): the final pulse of the Variscan Orogeny in the Bohemian Massif constrained by LA-SF-ICP-MS U-Pb zircon data. Geological Society Special Publications, **327**: 197–214; https://doi.org/10.1144/SP327.10

Imposa, S., Guidi, G.D., Grassi, S., Scudero, S., Barreca, G., Patti, G., Boso, D., 2015. Applying geophysical techniques to investigate a segment of a creeping fault in the urban area of San Gregorio di Catania, southern flank of Mt. Etna (Sicily, Italy). Journal of Applied Geophysics, **123**: 153–163; https://doi.org/10.1016/j.jappgeo.2015.10.008

Jastrzębski, M., Budzyń, B., Żelaźniewicz, A., Konečný, P., Sláma, J., Kozub-Budzyń, G.A., Skrzypek, E., Jaźwa, A., 2021. Eo-Variscan metamorphism in the Bohemian Massif: Thermodynamic modelling and monazite geochronology of gneisses and granulites of the Góry Sowie Massif, SW Poland. Journal of Metamorphic Geology, **39**: 751–779; https://doi.org/10.1111/jmg.12589

Jastrzębski, M., Żelaźniewicz, A., Sláma, J., Krzemińska, E., Śliwiński, M., 2025. The Eo-Variscan domain in the Variscan belt: New data from the Sudetes, southern Poland. Lithos, **504–505**, 108058; https://doi.org/10.1016/j.lithos.2025.108058

Keller, G.V., Frischknecht, F.C., 1966. Electrical Methods in Geophysical Prospecting. Elsevier Science & Technology.

Kemna, A., Vanderborght, J., Kulessa, B., Vereecken, H., 2002. Imaging and characterisation of subsurface solute transport using electrical resistivity tomography (ERT) and equivalent transport models. Journal of Hydrology, **267**: 125–146; https://doi.org/10.1016/S0022-1694(02)00145-2

Kley, J., Voigt, T., 2008. Late Cretaceous intraplate thrusting in central Europe: Effect of Africa-Iberia-Europe convergence, not Alpine collision. Geology, **36**: 839–842; https://doi.org/10.1130/G24930A.1

Kowalczyk, S., Zawrzykraj, P., Mieszkowski, R., 2015. Application of electrical resistivity tomography in assessing complex soil conditions. Geological Quarterly, **59** (3): 367–372; https://doi.org/10.7306/gq.1172

Kowalski, A., 2018. Landslides and the incorrect interpretation of geological structure – examples from the Sudety Mountains (in Polish with English summary). Biuletyn Państwowego Instytutu Geologicznego, **473**: 27–48; https://doi.org/10.5604/01.3001.0012.7708

Kowalski, A., 2020. Triassic palaeogeography of NE Bohemian Massif based on sedimentological record in the Wleń Graben and the Krzeszów Brachysyncline (SW Poland). Annales Societatis Geologorum Poloniae, **90**: 125–148; https://doi.org/10.14241/asgp.2020.09

Kowalski, A., 2021a. Late Cretaceous palaeogeography of NE Bohemian Massif: diachronous sedimentary successions in the Wleń Graben and Krzeszów Brachysyncline (SW Poland). Annales Societatis Geologorum Poloniae, **91**: 1–36; https://doi.org/10.14241/asgp.2021.05

Kowalski, A., 2021b. Multistage structural evolution of the end-Cretaceous–Cenozoic Wleń Graben (the Sudetes, NE Bohemian Massif) – a contribution to the post-Variscan tectonic history of SW Poland. Annales Societatis Geologorum Poloniae, **91**: 37–66; https://doi.org/10.14241/asgp.2020.21

Kowalski, A., 2024. Late- to post-Variscan structural evolution of tectonic grabens on top of the Góry Sowie Massif. In: 20th Jubilee Meeting of the Central European Tectonic Studies Groups CETEG, Srebrna Góra, 24-27.04.2024, Poland. Abstract Volume and Field Trips Guide: 153–182; https://doi.org/10.7306/CETEG2024-2

Kowalski, A., 2025. Karbońska pokrywa osadowa masywu Gór Sowich (in Polish). In: Krystaliczne podłoże i karbońskie baseny sedymentacyjne w masywie Gór Sowich (ed. A. Kowalski): 22–35. Materiały Konferencji Terenowej, Polskie Towarzystwo Geologiczne.

Kowalski, A., Pacanowski, G., 2025. A record of superimposed late- and post-Variscan regional-scale tectonic events at the NE margin of the Bohemian Massif: structural evolution of the Kamionki Graben (SW Poland, Sudetes). Geological Quarterly, 69, 6; https://doi.org/10.7306/gq.1779

Krautblatter, M., Hauck, C., 2007. Electrical resistivity tomography monitoring of permafrost in solid rock walls. Journal of Geophysical Research: Earth Surface, 112, F02S20; https://doi.org/10.1029/2006JF00054

Kröner, A., Hegner, E., 1998. Geochemistry, single zircon ages and Sm–Nd systematics of granitoid rocks from the Góry Sowie (Owl Mts), Polish West Sudetes: evidence for early arc-related plutonism. Journal of the Geological Society, 155: 711–724; https://doi.org/doi.org/10.1144/gsjgs.155.4.0711

Kryza, R., Fanning, C.M., 2007. Devonian deep-crustal metamorphism and exhumation in the Variscan Orogen: evidence from SHRIMP zircon ages from the HT-HP granulites and migmatites of the Góry Sowie (Polish Sudetes). Geodinamica Acta, 20: 159–175; https://doi.org/10.3166/ga.20.159-175

Krzyszkowski, D., Bowman, D., 1997. Neotectonic deformation of Pleistocene deposits along the Sudetic Marginal Fault, southwestern Poland. Earth Surface Processes and Landforms, 22: 545–562.

Krzyszkowski, D., Pijet, E., 1993. Morphological effects of Pleistocene fault activity in the Sowie Mts., southwestern Poland. Zeitschrift für Geomorphologie, 94: 243–259.

Krzyszkowski, D., Migoń, P., Sroka, W., 1995. Neotectonic Quaternary history of the Sudetic Marginal Fault, SW Poland. Folia Quaternaria: 66: 73–98.

Krzywiec, P., Mazur, S., Gągała, Ł., Kufrasa, M., Lewandowski, M., Malinowski, M., Buffenmyer, V., 2017. Late Carboniferous thin-skinned compressional deformation above the SW edge of the East European craton as revealed by seismic reflection and potential field data—Correlations with the Variscides and the Appalachians. GSA Memoir, 213: 353–372; https://doi.org/10.1130/2017.1213(14)

Kurochkina, L.Y., Osiptsov, A.A., Tsvelodub, O.Yu., 2008. Statistical features of the transport properties of multiscale isotropic porous media. Journal of Engineering Physics and Thermophysics, 81: 875–883; https://doi.org/10.1007/s10891-008-0156-7

Loke, M., Alfouzan, F.A., Nawawi, M., 2007. Optimisation of electrode arrays used in 2D resistivity imaging surveys. ASEG Extended Abstracts, 1: 1–4; https://doi.org/10.1071/ASEG2007ab002

Loke, M.H., 2000. Electrical Imaging Syrveys for Environmental and Engineering Studies. A Practical Guide to 2-D and 3-D Surveys, Geotomo, Malaysia.

Loke, M.H., 2012. Tutorial: 2-D and 3-D Electrical Imaging Surveys. Geotomo Software, Malaysia; https://refhub.elsevier.com/S0926-9851(18)31023-1/rf0365

Loke, M.H., Barker, R.D., 1996. Rapid least-squares inversion of apparent resistivity pseudosections by a quasi-Newton method. Geophysical Prospecting, 44: 131–152; https://doi.org/10.1111/j.1365-2478.1996.tb00142.x

Łapot, W., 1986. Petrography of Carboniferous rocks from the Sowie Mts. (in Polish with English summary). Geologia Sudetica, 21: 1–144.

Łapot, W., 1988. Petrography of the Sowie Mts. Kulm. Bulletin of the Polish Academy of Sciences, Earth Sciences, 36: 183–195.

Martínez-Catalán, J.R., Schulmann, K., Ghienne, J.-F., 2021. The Mid-Variscan Allochthon: Keys from correlation, partial retrodeformation and plate-tectonic reconstruction to unlock the geometry of a non-cylindrical belt. Earth-Science Reviews, 220, 103700; https://doi.org/10.1016/j.earscirev.2021.103700

Mazur, S., Puziewicz, J., 1995. Mylonites of the Niemcza Fault Zone (in Polish with English summary). Annales Societatis Geologorum Poloniae, 64: 23–52.

Mazur, S., Schulmann, K., 2025. At the border of peri-Gondwana and Baltica: the structure of the eastern termination of the Variscan belt. Journal of the Geological Society, 182, jgs2024-075; https://doi.org/10.1144/jgs2024-075

Mazur, S., Scheck-Wenderoth, M., Krzywiec, P., 2005. Different modes of the Late Cretaceous–Early Tertiary inversion in the North German and Polish basins. International Journal of Earth Sciences, 94: 782–798; https://doi.org/10.1007/s00531-005-0016-z

Mazur, S., Aleksandrowski, P., Kryza, R., Oberc-Dziedzic, T., 2006. The Variscan Orogen in Poland. Geological Quarterly, 50 (1): 89–118.

Mazur, S., Aleksandrowski, P., Turniak, K., Krzemiński, L., Mastalerz, K., Górecka-Nowak, A., Kurowski, L., Krzywiec, P., Żelaźniewicz, A., Fanning, M., 2010. Uplift and late orogenic deformation of the Central European Variscan belt as revealed by sediment provenance and structural record in the Carboniferous foreland basin of western Poland. International Journal of Earth Sciences, 99: 47–64; https://doi.org/10.1007/s00531-008-0367-3

Mazur, S., Turniak, K., Szczepański, J., McNaughton, N.J., 2015. Vestiges of Saxothuringian crust in the Central Sudetes, Bohemian Massif: Zircon evidence of a recycled subducted slab provenance. Gondwana Research, 27: 825–839; https://doi.org/10.1016/j.gr.2013.11.005

Mazur, S., Aleksandrowski, P., Gągała, Ł., Krzywiec, P., Żaba, J., Gaidzik, K., Sikora, R., 2020. Late Palaeozoic strike-slip tectonics versus oroclinal bending at the SW outskirts of Baltica: case of the Variscan belt's eastern end in Poland. International Journal of Earth Sciences, 109: 1133–1160; https://doi.org/10.1007/s00531-019-01814-7

Migoń, P., Łach, J., 1998. Geomorphological evidence of neotectonics in the Kaczawa sector of the Sudetic Marginal Fault, southwestern Poland. Geologia Sudetica, 31: 307–316.

Migoń, P., Latocha-Wites, A., Jancewicz, K., 2023. Geomorphology of the Sowie Mountains (Sudetes, SW Poland) – landform patterns and anthropogenic impact. Geographia Polonica, 96: 103–129; https://doi.org/10.7163/GPol.0248

Mojica, A., Pérez, T., Toral, J., Miranda, R., Franceschi, P., Calderón, C., Vergara, F., 2017. Shallow electrical resistivity imaging of the Limón fault, Chagres River Watershed, Panama Canal. Journal of Applied Geophysics, 138: 135–142; https://doi.org/10.1016/j.jappgeo.2017.01.010

Mroczkowski, J., Mader, D., 1985. Sandy inland braidplain deposition with local aeolian sedimentation in the lower and middle parts of the Buntsandstein and sandy coastal braidplain deposition in the topmost Zechstein in the Sudetes (Lower Silesia, Poland). In: Aspects of Fluvial Sedimentation in the Lower Triassic Buntsandstein of Europe (ed. D. Mader): 165–195. Springer, Berlin.

Müller, K., Polom, U., Winsemann, J., Steffen, H., Tsukamoto, S., Günther, T., Igel, J., Spies, T., Lege, T., Frechen, M., Franzke, H.J., Brandes, C., 2020. Structural style and neotectonic activity along the Harz Boundary Fault, northern Germany: a multimethod approach integrating geophysics, outcrop data and numerical simulations. International Journal of Earth Sciences, 109: 1811–1835; https://doi.org/10.1007/s00531-020-01874-0

Muszer, J., Górecka-Nowak, A., Kryza, R., August, C., 2016. New data on biostratigraphy and chronostratigraphy of the Carboniferous sediments in Sudetes (in Polish). In: XXIII Konferencja Naukowa Sekcji Paleontologicznej Polskiego Towarzystwa Geologicznego (eds. K. Pawłowska and D. Pawłowski) : 73–74.

Nádaskay, R., Žák, J., Sláma, J., Sidorinová, T., Valečka, J., 2019. Deciphering the Late Paleozoic to Mesozoic tectono sedimentary evolution of the northern Bohemian Massif from detrital zircon geochronology and heavy mineral provenance. International Journal of Earth Sciences, 108: 2653–2681; https://doi.org/10.1007/s00531-019-01781-z

Nádaskay, R., Valečka, J., Opluštil, S., Mlčoch, B., Skácelová, Z., Horna, F., 2024. Pennsylvanian–Permian deposits in northern Bohemia: a correlation with neighbouring basins and discussion of their formation and demise within the "Elbe Zone System". Geological Quarterly, **68**, 42; https://doi.org/10.7306/gq.1770

Narkiewicz, M., 2007. Development and inversion of Devonian and Carboniferous basins in the eastern part of the Variscan foreland (Poland). Geological Quarterly, **51** (1): 231–256.

Narkiewicz, M., 2020. Variscan foreland in Poland revisited: new data and new concepts. Geological Quarterly, **64** (2): 377–401; https://doi.org/10.7306/gq.1511

NASA, 2001. Shuttle Radar Topography Mission (SRTM) 1 Arc-Second Global. Distributed by the Land Processes Distributed Active Archive Center (LP DAAC), U.S. Geological Survey; https://lpdaac.usgs.gov/

Nemec, W., Porębski, S.J., Teisseyre, A.K., 1982. Explanatory notes to the lithotectonic molasse profile of the Intra-Sudetic Basin, Polish part (Sudety Mts., Carboniferous-Permian). Veröffentlichungen des Zentralinstituts für Physik der Erde, **66**: 267–278.

Novakova, L., 2015. Tectonic phase separation applied to the Sudetic Marginal Fault Zone (NE part of the Czech Republic). Journal of Mountain Science, **12**: 251–267; https://doi.org/10.1007/s11629-014-3297-5

Oberc, J., 1949. Zagadnienia geologiczne kulmu sowiogórskiego (in Polish). Sprawozdania Poznańskiego Towarzystwa Przyjaciół Nauk, 1: 159–162.

Oberc, J., 1972. Sudety i obszary przyległe (in Polish). In: W. Pożaryski (Ed.), Budowa Geologiczna Polski. Vol. 4. Tektonika, Part 2. Wydaw. Geol., Warszawa.

Oberc, J., Dyjor, S., 1969. Sudetic Marginal Fault (in Polish with English summary). Biuletyn Instytutu Geologicznego, **236**: 41–142.

O'Brien, P.J., Kröner, A., Jaeckel, P., Hegner, E., Żelaźniewicz, A., Kryza, R., 1997. Petrological and isotopic studies on Palaeozoic high-pressure granulites, Gory Sowie Mts, Polish Sudetes. Journal of Petrology, **38**: 433–456; https://doi.org/10.1093/petroj/38.4.433

Ostrowski, S., Lasocki, M., Pacanowski, G., 2010. Electrical resistivity tomography as a tool in geological mapping. In: 72nd EAGE Conference and Exhibition incorporating SPE EUROPEC 2010. European Association of Geoscientists & Engineers, cp-161.

Ostrowski, S., Pacanowski, G., Majer, E., Sokołowska, M., Czarniak, P., Piechota, A., Barański, M., Szabłowska, M., Lasocki, M., Wilkołazki, P., Majer, K., 2023. Badania geologiczno-inżynierskie. Geofizyka inżynierska (in Polish). Państw. Inst. Geol. – PIB, Warszawa.

Ostrowski, S., Bąk, T., Czarniak, P., Lasocki, M., Pacanowski, G., Sobótka, P., 2022. Dokumentacja badań geofizycznych wykonana metodą tomografii elektrooporowej (ERT) i sejsmiki refrakcyjnej (SRT-P) w ramach reambulacji Szczegółowej Mapy Geologicznej Sudetów w skali 1:25 000, arkusz Walim, gm. Walim, pow. wałbrzyski, woj. dolnośląskie, PIG-PIB Warszawa (in Polish). Arch. CAG PIG, Warszawa CBDG: 1711235.

Pacanowski, G., Maślakowski, M., Lejzerowicz, A., 2021. Practical aspects of field work carried out by Electrical Resistivity Tomography. Archives of Civil Engineering, **68**: 331–346; https://doi.org/10.24425/ace.2022.143041

Perrone, A., Lapenna, V., Piscitelli, S., 2014. Electrical resistivity tomography technique for landslide investigation: A review. Earth-Science Reviews, **135**: 65–82; https://doi.org/10.1016/j.earscirev.2014.04.002

Pešková, I., Hók, J., Štěpančíková, P., Stemberk, J., Vojtko, R., 2010. Results of stress analysis inferred from fault slip data along the Sudetic Marginal Fault (NE part of Bohemian Massif). Acta Geologica Slovaca, **2**: 11–16.

Petit, J.P., 1987. Criteria for the sense of movement on fault surfaces in brittle rocks. Journal of Structural Geology, **9**: 597–608; https://doi.org/10.1016/0191-8141(87)90145-3

Pietranik, A., Storey, C., Kierczak, J., 2013. Niemcza diorites and monzodiorites (Sudetes, SW Poland): a record of changing geotectonic setting at ca. 340 Ma. Geological Quarterly, **57** (3): 325–334; https://doi.org/10.7306/gq.1084

Porębski, S.J., 1981. Świebodzice succesion (Upper Devonian-lowest Carboniferous): a prograding, mass flow dominated fan-delta complex (in Polish with English summary). Geologia Sudetica, **21**: 101–192.

Porębski, S.J., 1990. Onset of coarse clastic sedimentation in the Variscan realm of the Sudetes (SW Poland): an example from the upper Devonian-lower Carboniferous Świebodzice succession. Neues Jahrbuch für Geologie und Paläontologie Abhandlungen, **179**: 259–274.

Porras, D., Carrasco, J., Carrasco, P., González, P.J., 2022. Imaging extensional fault systems using deep electrical resistivity tomography: A case study of the Baza fault, Betic Cordillera, Spain. Journal of Applied Geophysics, **202**, 104673; https://doi.org/10.1016/j.jappgeo.2022.104673

Putiška, R., Nikolaj, M., Dostál, I., Kušnirák, D., 2012. Determination of cavities using electrical resistivity tomography. Contributions to Geophysics and Geodesy, **42**: 201–211.

Racki, G., Mazur, S., Narkiewicz, K., Pisarzowska, A., Bardziński, W., Kołtonik, K., Szymanowski, D., Filipiak, P., Kremer, B., 2022. A waning Saxothuringian Ocean evidenced in the Famennian tephra-bearing siliceous succession of the Bardo Unit (Central Sudetes, SW Poland). GSA Bulletin, **134**: 2373–2398; https://doi.org/10.1130/B35971.1

Reynolds, J.M., 2011. An Introduction to Applied and Environmental Geophysics (2nd ed.). John Wiley & Sons.

Rosenbaum, G., Lister, G.S., Duboz, C., 2002. Relative motions of Africa, Iberia and Europe during Alpine orogeny. Tectonophysics, **359**: 117–129; https://doi.org/10.1016/S0040-1951(02)00442-0

Różycka, M., Jancewicz, K., Migoń, P., Szymanowski, M., 2021. Tectonic versus rock-controlled mountain fronts – Geomorphometric and geostatistical approach (Sowie Mts., Central Europe). Geomorphology, **373**, 107485; https://doi.org/10.1016/j.geomorph.2020.107485

Sawicki, L., 1995. Geological Map of Lower Silesia with Adjacent Czech and German Territories (without Quaternary deposits). Państw. Inst. Geol., Warszawa.

Schulmann, K., Edel, J.B., Catalán, J.R.M., Mazur, S., Guy, A., Lardeaux, J.M., Ayarza, P., Palomeras, I., 2022. Tectonic evolution and global crustal architecture of the European Variscan belt constrained by geophysical data. Earth-Science Reviews, **234**, 104195; https://doi.org/10.1016/j.earscirev.2022.104195

Šilhán, K., Pánek, T., 2010. Fossil and recent debris flows in medium–high mountains (Moravskoslezské Beskydy Mts, Czech Republic). Geomorphology, **124**: 238–249; https://doi.org/10.1016/j.geomorph.2010.03.026

Sobczyk, A., Szczygieł, J., 2021. Paleostress reconstruction of faults recorded in the Niedźwiedzia Cave (Sudetes): insights into Alpine intraplate tectonic of NE Bohemian Massif. International Journal of Earth Sciences, **110**: 833–847; https://doi.org/10.1007/s00531-021-01994-1

Sobczyk, A., Danišík, M., Aleksandrowski, P., Anczkiewicz, A., 2015. Post-Variscan cooling history of the central Western Sudetes (NE Bohemian Massif, Poland) constrained by apatite fission-track and zircon (U-Th)/He thermochronology. Tectonophysics, **649**: 47–57; https://doi.org/10.1016/j.tecto.2015.02.021

Sobczyk, A., Sobel, E., Georgieva, V., 2019. Meso–Cenozoic cooling and exhumation history of the Orlica-Śnieżnik Dome (Sudetes, NE Bohemian Massif, Central Europe): Insights from apatite fission-track thermochronometry. Terra Nova, **32**: 122–133; https://doi.org/10.1111/ter.12449

Solecki, A.T., 1994. Tectonics of the North Sudetic Synclinorium. Acta Universitatis Wratislaviensis, **45**: 1–59.

Solecki, A.T., 2011. Structural development of the epi-Variscan cover in the North Sudetic Synclinorium area (in Polish with English summary). In: Mezozoik i kenozoik Dolnego Śląska (eds. A. Żelaźniewicz, J. Wojewoda and W. Cieżkowski): 19–36. LXXXI Zjazdu Polskiego Towarzystwa Geologicznego. WIND.

SPDPSH (System Przetwarzania Danych Państwowej Służby Hydrogeologicznej), 2025. Centralny Bank Danych Hydrogeologicznych (in Polish); https://www.pgi.gov.pl/psh/dane-hydrogeologiczne-psh/947-bazy-danych-hydrogeologiczne/9057-bankhydro.html, accessed: 20-05-2025.

Štěpančíková, P., Hók, J., Nývlt, D., Dohnal, J., Sýkorová, I., Stemberk, J., 2010. Active tectonics research using trenching technique on the south-eastern section of the Sudetic Marginal Fault (NE Bohemian Massif, central Europe). Tectonophysics, **485**: 269–282; https://doi.org/10.1016/j.tecto.2010

Štěpančíková, P., Dohnal, J., Pánek, T., Łój, M., Smolková, V., Šilhán, K., 2011. The application of electrical resistivity tomography and gravimetric survey as useful tools in an active tectonics study of the Sudetic Marginal Fault (Bohemian Massif, central Europe). Journal of Applied Geophysics, **74**: 69–80; https://doi.org/10.1016/j.jappgeo.2011.03.007

Štěpančíková, P., Stemberk, J., Tábořík, P., Fischer, T., Findžová, L., Valenta, J., 2025. Discovering the Čirá–Kopanina Fault: Bridging the Gap between Surface Evidence and Seismic Activity. Lithosphere, **15**, 192; https://doi.org/10.2113/2024/lithosphere_2024_192.01.004

Suzuki, K., Toda, S., Kusunoki, K., Fujimitsu, Y., Mogi, T., Jomori, A., 2000. Case studies of electrical and electromagnetic methods applied to mapping active faults beneath the thick quaternary. Engineering Geology, **56**: 29–45; https://doi.org/10.1016/S0013-7952(99)00132-5

Tabaud, A.S., Štípská, P., Mazur, S., Schulmann, K., Míková, J., Wong, J., Sun, M., 2021. Evolution of a Cambro-Ordovician active margin in northern Gondwana: Geochemical and zircon geochronological evidence from the Góry Sowie metasedimentary rocks, Poland. Gondwana Research, **90**: 1–26; https://doi.org/10.1016/j.gr.2020.10.011

Teisseyre, H., Sawicki, L., 1958. Szczegółowa Mapa Geologiczna Sudetów w skali 1:25 000, arkusz Zagórze Śląskie (in Polish). Wadaw. Geol., Warszawa.

Tomaszczyk, M., Jarosiński, M., 2017. The Kock Fault Zone as an indicator of tectonic stress regime changes at the margin of the East European Craton (Poland). Geological Quarterly, **61** (4): 908–925; https://doi.org/10.7306/gq.1380

Tomek, F., Vacek, F., Žák, J., Petronis, M.S., Verner, K., Foucher, M.S., 2019. Polykinematic foreland basins initiated during orthogonal convergence and terminated by orogen-oblique strike-slip faulting: An example from the northeastern Variscan belt. Tectonophysics, **766**: 379–397; https://doi.org/10.1016/j.tecto.2019.05.023

Topolewska, S., Stępień, M., Kowalczyk, S., 2016. Mapping of the north-eastern part of Kozłowicka buried valley based on geoelectrical data. Studia Quaternaria, **33**: 91–101; https://doi.org/10.1515/squa-2016-0009

Valečka, J., 2019. Jurassic pebbles in the Cretaceous sandstones of the Bohemian Basin as a possible tool for the reconstruction of Late Jurassic and Late Cretaceous paleogeography. Volumina Jurassica, **18**: 17–38; https://doi.org/10.7306/vj.17.2

Van Breemen, O., Bowes, D., Aftalion, M., Żelaźniewicz, A., 1988. Devonian tectonothermal activity in the Sowie Góry gneissic block, Sudetes, southwestern Poland: evidence from Rb-Sr and U-Pb isotopic studies. Annales Societatis Geologorum Poloniae, **58**: 3–19.

Voigt, T., 2009. Die Lausitzer-Riesengebirgs Antiklinalzone als kreidezeitliche inversionsstruktur: geologische Hinweise aus den umgebenden Kreidebecken. Zeitschrift für Geologische Wissenschaften, **37**: 15–39.

Voigt, T., Kley, J., Voigt, S., 2021. Dawn and dusk of Late Cretaceous basin inversion in central Europe. Solid Earth, **12**: 1443–1471; https://doi.org/10.5194/se-12-1443-2021

Wajsprych, B., 1978. Allochthonous Paleozoic rocks in the Visean of the Bardzkie Mts. (Sudetes) (in Polish with English summary). Annales Societatis Geologorum Poloniae, **48**: 99–127.

Węzyk, P., 2015 (ed.). Handbook for participants training in the use of LiDAR products (in Polish). Informatyczny System Osłony Kraju przed nadzwyczajnymi zagrożeniami. Główny Urząd Geodezji i Kartografii, Warszawa.

Wojewoda, J., 1997. Upper Cretaceous littoral-to-shelf succession in the Intrasudetic Basin and Nysa Trough, Sudety Mts. In: Obszary Źródłowe: Zapis w Osadach, **1**: 81–96.

Wojtulek, P.M., Schulz, B., Klemd, R., Gil, G., Dajek, M., Delura, K., 2022. The Central-Sudetic ophiolites – Remnants of the SSZ-type Devonian oceanic lithosphere in the European part of the Variscan Orogen. Gondwana Research, **105**: 343–365; https://doi.org/10.1016/j.gr.2021.09.015

Woźniak, T., Bania, G., Mościcki, W.J., Ćwiklik, M., 2018. Electrical resistivity tomography (ERT) and sedimentological analysis applied to investigation of Upper Jurassic limestones from the Krzeszowice Graben (Kraków Upland, southern Poland). Geological Quarterly, **62** (2): 287–302; https://doi.org/10.7306/gq.1403

Zhou, Q.Y., Shimada, J., Sato, A., 2001. Three-dimensional spatial and temporal monitoring of soil water content using electrical resistivity tomography. Water Resources Research, **37**: 273–285; https://doi.org/10.1029/2000WR900284

Zhou, W., Beck, B.F., Adams, A.L., 2002. Effective electrode array in mapping karst hazards in electrical resistivity tomography. Environmental Geology, **42**: 922–928; https://doi.org/10.1007/s00254-002-0594-z

Zhu, T., Feng, R., Hao, J., Zhou, J., Wang, H., Wang, S., 2009. The Application of Electrical Resistivity Tomography to Detecting a Buried Fault: A Case Study. Journal of Environmental and Engineering Geophysics, **14**: 145–151; https://doi.org/10.2113/JEEG14.3.145

Žák, J., Svojtka, M., Opluštil, S., 2018. Topographic inversion and changes in the sediment routing systems in the Variscan orogenic belt as revealed by detrital zircon and monazite UPb geochronology in post-collisional continental basins. Sedimentary Geology, **377**: 63–81; https://doi.org/10.1016/j.sedgeo.2018.09.008

Żakowa, H., 1959. Opracowanie stratygraficzne utworów morskich dolnego karbonu w okolicy Glinna (in Polish). Arch. CAG PIG, Wrocław, CBDG: 1191751.

Żakowa, H., 1960. Horizon *Goniatites crenistria* from Glinno (Sowie Góry, Sudeten Mts.) (in Polish with English summary). Kwartalnik Geologiczny, **4** (3): 349–366.

Żakowa, H., 1963. Stratigraphy and facial extents of the Lower Carboniferous in the Sudetes (in Polish with English summary). Kwartalnik Geologiczny, **7** (1): 73–94.

Żakowa, H., 1966. Zone *Goniatites crenistria* Phill. in the vicinity of Sokolec and Jugów, at the foot of the Sowie Mountains (Central Sudetes) (in Polish with English summary). Prace Instytutu Geologicznego, **43**.

Żakowa, H., Żak, C., 1962. Lower Carboniferous at Kamionki (Sowie Mts. – Lower Silesia) (in Polish with English summary). Biuletyn Instytutu Geologicznego, **173**: 169–277.

Żelaźniewicz, A., 1987. Tectonic and metamorphic evolution of the Sowie Góry, Sudetes Mts., SW Poland (in Polish with English summary). Annales Societatis Geologorum Poloniae, **57**: 203–348.

Żelaźniewicz, A., 1990. Deformation and metamorphism in the Góry Sowie gneiss complex, Sudetes, SW Poland. Neues Jahrbuch für Geologie und Paläontologie Abhandlungen, **179**: 129–157.

Żelaźniewicz, A., Cwojdziński, S., England, R.W., Zientara, P., 1997. Variscides in the Sudetes and the reworked Cadomian orogen: evidence from the GB-2A seismic reflection profiling in southwestern Poland. Geological Quarterly, **41** (2): 289–308.